

Structural Behavior of the Peptaibol Harzianin HK VI in a DMPC Bilayer: Insights from MD Simulations

Marina Putzu,¹ Sezgin Kara,² Sergii Afonin,³ Stephan L. Grage,³ Andrea Bordessa,⁴ Grégory Chaume,⁴ Thierry Brigaud,⁴ Anne S. Ulrich,^{2,3} and Tomáš Kubar^{1,*}

¹Center for Functional Nanostructures and Institute of Physical Chemistry, ²Institute of Organic Chemistry, and ³Institute of Biological Interfaces (IBG-2), Karlsruhe Institute of Technology, Karlsruhe, Germany; and ⁴Laboratoire de Chimie Biologique (LCB), EA 4505, Université de Cergy-Pontoise, Neuville sur Oise, Cergy-Pontoise Cedex, France

ABSTRACT Microsecond molecular dynamics simulations of harzianin HK VI (HZ) interacting with a dimyristoylphosphatidylcholine bilayer were performed at the condition of low peptide-to-lipid ratio. Two orientations of HZ molecule in the bilayer were found and characterized. In the orientation perpendicular to the bilayer surface, HZ induces a local thinning of the bilayer. When inserted into the bilayer parallel to its surface, HZ is located nearly completely within the hydrophobic region of the bilayer. A combination of solid-state NMR and circular dichroism experiments found the latter orientation to be dominant. An extended sampling simulation provided qualitative results and showed the same orientation to be a global minimum of free energy. The secondary structure of HZ was characterized, and it was found to be located in the 3_{10} -helical family. The specific challenges of computer simulation of nonpolar peptides are discussed briefly.

INTRODUCTION

Peptaibols

Peptaibols are a special class of short peptides with a length from seven to twenty amino acids (AA), significant content of noncanonical α -tetrasubstituted residues like the aminoisobutyric acid (Aib), alkylated N-terminus, and a C-terminal 1,2-amino alcohol group (1). Largely hydrophobic and proteolytically stable, nonribosomally produced peptaibols are secondary metabolites in soil filamentous fungi and demonstrate pronounced antibiotic, antifungal, and anticancer activities, which render them as potentially interesting leads for pharmacological and agricultural applications. Peptaibols are uniformly membrane-active compounds, and like many other membranolytic peptides, they are believed to exert their activity mostly via a pore formation in targeted biomembranes. In this connection, peptaibols are particularly intriguing membrane-active peptides (MAP) because many of them indeed show membrane voltage activation and formation of ionic channels in artificial lipid bilayers. Hence, peptaibols have been much investigated as model systems for voltage-gated phenomena.

The backbone of a peptaibol molecule generally forms a helical structure due to the conformational constraints

imposed by the presence of abundant Aib (2). Homooligomeric Aib peptides prefer the 3_{10} -helical conformation whereas either α - or mixed-helical conformations prevail whenever Aib is incorporated as a guest residue in host polypeptides (3–6). Furthermore, the helix-stabilizing effect of Aib in a foreign sequence even overrides the effects of helix-breaking AAs (3). Peptaibols are classified into: 1) long-sequence peptaibols (18–20 AA, typically with a centrally located Pro, and Gln residues near both termini); 2) short-sequence peptaibols (11–16 AA, with several Aib-Pro motives, and typically either Ac-Aib-Asn- or Ac-Aib-Gln- as N-terminus); and 3) ultrashort lipopeptaibols (7 or 11 AA, with a high content in Gly and N-terminal AA acylated by a C8–C15 fatty acid).

The archetypal representatives of the long-sequence peptaibols are alamethicins (ALM). The most studied variant ALM F30/3 (Ac-Aib-Pro-Aib-Ala-Aib-Ala-Gln-Aib-Val-Aib-Gly-Leu-Aib-Pro-Val-Aib-Aib-Glu-Gln-Pheol) forms amphipathic α -helices, which assemble into stable ion channels with well-defined conductance levels, and its resultant cytolytic activity was recognized already in the 1960s (7). ALM may either bind to the surface of a lipid bilayer, or it may penetrate into the interior of the bilayer; as soon as inserted, it may form oligomers and, thus, create barrel-stave or helix-bundle channels (8,9), which may be filled with water and conduct ions consequently. Short-sequence peptaibols were also reported to form pores and channels

Submitted December 14, 2016, and accepted for publication May 12, 2017.

*Correspondence: tomas.kubar@kit.edu

Editor: Bert de Groot.

<http://dx.doi.org/10.1016/j.bpj.2017.05.019>

© 2017 Biophysical Society.

on planar lipid bilayer membranes (10). However, most of the studies of short-sequence peptaibols have focused on solution structural features, and not so much is known as for the behavior of these peptaibols inside a membrane. On the contrary, lipopeptaibols received more attention with regard to the membrane-inserted structure. Representative is the lipopeptaibol trichogin GA IV of the sequence nOct-Aib-Gly-Leu-Aib-Gly-Gly-Leu-Aib-Gly-Ile-Leuol (11).

Harzianin HK VI

The subject of this work is the short-sequence peptaibol harzianin HK VI (hereafter called “HZ”). HZ is produced naturally by various terrestrial and marine fungi of the *Trichoderma sp.*, and was first isolated from *T. pseudokoningii* and characterized by Rebuffat et al. (12) in 1996. Within its 11-residue sequence, Ac-Aib-Asn-Ile-Ile-Aib-Pro-Leu-Leu-Aib-Pro-Leuol, HZ contains two Aib-Pro pairs at positions 5–6 and 9–10, the Ac-Aib-Asn run at the N-terminus, and several bulky hydrophobic Leu/Ile residues. Notably, due to mass spectrometry being the prime sequencing method, inability to distinguish Leu from Ile leads to the ambiguity in identification of HZ analogs, e.g., when Lxx is reported as an aliphatic residue.

Functional studies showed HZ, its homologs (Ac-Aib-Asn-Lxx-Lxx-Aib-Pro-Lxx-Lxx-Aib-Pro-Lxxol), or mixtures containing HZ to exert embryotoxicity against *Crassostrea gigas* (13) as well as chlorpromazine-level neuroleptic effects in male mice (14). Crude extracts from HZ-producing fungi inhibited motility of the boar spermatozoa and quenched the mitochondrial transmembrane potential of the sperm cells at low exposure concentrations (14,15). HZ is a membrane-active peptaibol as it was reported to cause leakage of the carboxyfluorescein-loaded lecithin/cholesterol liposomes and, as other short-sequence peptaibols, forms pores and channels on planar lipid bilayer membranes (10,12,15). HZ can act as a cell-penetrating peptide—uptake of covalently conjugated oligonucleotides was shown (16,17).

Notably, there are no particularly strong in vitro cytotoxic effects demonstrated specifically for HZ or any other short-sequence peptaibols. Taken together with the fact that peptaibols are produced in mixtures as natural combinatorial libraries, this finding challenges putative exclusive membranolytic cytotoxicity as a prime mechanism of biological action and the main purpose of their biosynthetic production. Particularly interesting as alternatives are recently suggested synergies between hydrolytic enzymes and membrane-affecting peptaibols indirectly leading to concerted fungicidal effects (18). Furthermore, a 2012 article by Mikkola et al. (15) proposes the synergistic enhancement of the membrane-permeabilizing activity of canonical 20-mer peptaibols (like ALM) by the 11-mer ones, i.e., by the short-sequence peptaibols like HZ. Should any of these alternatives or the direct membranolytic action be the prime

mechanism of HZ biological action, determination of HZ structure in the membrane-bound state is of key relevance.

From the general structure perspective, all harzianins (and their sequential analogs) including HZ were suggested to assume a β -bend ribbon spiral secondary structure, based on partial NMR structural studies of HZ and compositional homology to other (longer) harzianins. The β -bend ribbon conformation with backbone torsion angles as in Table 1 (19) was determined in MeOH using CD, molecular modeling, and NMR for the 14-mer harzianin HC IX. For this harzianin, the β -bend ribbon spiral was stabilized by type 1 \leftarrow 4 intramolecular H-bonds, some of which were absent in accordance with the presence of three Pro residues interrupting the hydrogen-bonding (H-bonding) network. The β -bend ribbon structure is logically projected to all (Aib-Pro)_n- and Xaa-Yaa-Aib-Pro-containing peptides in parallel to the expectation of a 3_{10} -helix for any oligo-Aib sequence. (Both compositional characteristics are present in HZ.) At the same time, an α -helical assumption appears not to be relevant for HZ, as it seems to prevail only for Aib-poor long-sequence peptaibols like ALMs.

Simulation of membrane-active peptides

Molecular dynamics (MD) simulation has been a useful tool for the investigation of MAPs for two decades. A comprehensive how-to on MD simulations of membrane proteins by Kandt et al. (20) and a short review by Lindahl and Sansom (21) cover also MAPs. MD simulations of MAPs face multiple challenges regarding the parametrization of lipids or more generally the development of force fields uniform for bilayers and molecules embedded into them, or the principal limitations of potential energy functions lacking electronic polarizability (22–24). Even if these challenges are tackled, there is a real danger of undersampling in all-atom MD simulations of even simple peptide-bilayer systems, as noted in the late 1990s already (25–27), and discussed, e.g., in Lindahl and Sansom (21). The reason is that the hydrocarbon tails of lipids rearrange very slowly; as an illustration, note the (lateral) diffusion coefficient in DMPC of 1–10 $\mu\text{m}^2/\text{s}$ (28,29), as compared to the value for water of 2000–3000 $\mu\text{m}^2/\text{s}$ (30).

A partial solution of this problem is to pass to coarse-grained (CG) representation (31), e.g., with the Martini force field (32), which improves the sampling by a factor of 100–1000. That makes CG simulation undoubtedly

TABLE 1 Backbone Dihedral Angles of the Fragment Forming a β -bend Ribbon Spiral Structure

Residue	φ	ψ
Xaa (<i>i</i>)	(−90 ± 8)°	(−27 ± 18)°
Yaa (<i>i</i> + 1)	(−98 ± 11)°	(−17 ± 14)°
Aib (<i>i</i> + 2)	(−49 ± 3)°	(−50 ± 1)°
Pro (<i>i</i> + 3)	(−78 ± 1)°	(+3 ± 19)°

Data is from Ségalas et al. (19).

useful for the initial docking and refinement of orientation with low resolution at least, whereas the lower level of detail may be of limited use for complex lipid environments, specific interactions, and fine conformational changes (31).

A promising simulation strategy seems to be to combine CG and all-atom representations for large-scale sampling and more detailed description of relevant structural states, respectively, to take advantage of the strengths of both of the approaches, as described by Rzeplia et al. (33). Parton et al. (34) exploited such a multiscale idea, starting with a CG simulation, then converting to an all-atom representation, and simulating further with an all-atom force field. Similarly, studying antimicrobial lipopeptides, Horn et al. (35) applied all-atom simulations to characterize the structural perturbation of the membrane, whereas they examined the (slow) process of binding to the membrane with a CG model (36).

Generally, the reliability and suitability of MD simulation should be tested by comparison with the outcome of biophysical experiments, like in the dedicated study by Wang et al. (37). The factors that affected the quality of the results were mostly the choice of the force field and the simulation parameters like inclusion or omission of counterions and the treatment of long-range electrostatics. These important topics were discussed also in other publications (38,39).

MAPs have been also a subject of work applying advanced simulation techniques. The temperature replica exchange protocol (replica-exchange MD) (40) was exploited in structural studies (41–44). The dissipative particle dynamics (45), which is a variant of CG MD, was applied in a study of pore formation and other bilayer deformations caused by several different MAPs (46). Umbrella sampling with a novel reaction coordinate was used in a work on antimicrobial lipopeptides forming a micelle and fusing with a membrane (47). Finally, a series of modern techniques were employed in a thermodynamic study of the WALP peptide (48): replica-exchange MD was combined with metadynamics with newly designed collective variables to yield the free energy of folding, and CG simulations used the Hamiltonian replica-exchange approach (HREX). These studies illustrate the flexibility and the broad range of options available for MD simulations of peptide/bilayer complexes.

Simulation of peptaibols

Approaching the topic of this work, MD simulations were previously employed to investigate the interaction of the long-sequence peptaibol ALM with lipid bilayers mostly consisting of POPC. Sometimes, ALM channels were built artificially first, and then simulated over tens of nanoseconds. The stability and dynamics properties of the helical bundles, the secondary structural elements, as well as the intra- and intermolecular H-bonding patterns were examined. First, rather short, all-atom simulations concentrated on a single ALM molecule, its structural stability, and insertion pathway (27,49), and the latter point was analyzed in

longer simulations (50). Further studied was the aggregation of several ALM molecules to form channels (51), a complex topic that was also approached with a combination of CG and all-atom simulations (52). The formation of aggregates was simulated on a CG level, and then all-atom simulations were applied to focus on the secondary structure of ALM as well as the interaction of water with the ALM clusters. The structure of the clusters was rather irregular, different from previous suggestions of symmetric channels formed by perfect α -helices. The observations would not have been possible with either CG or all-atom simulations alone.

Regarding short-sequence peptaibols, of which HZ is a representative, not much simulation work seems to have been done. Merely conformational analyses of short-sequence peptaibols in aqueous solution were reported, investigating trichobranchin A and B (53) and hypomurocin A (54). Further, an MD simulation study of the lipopeptaibol trichogin GA IV showed that such a short lipidated molecule interacts better with bilayers that are thinner by themselves, or, alternatively, the binding of the lipopeptaibol may induce local thinning of the membrane (55). It was noted, however, that the extent of simulation was insufficient to obtain global thermodynamics equilibrium due to the slow lateral diffusion of the lipid.

Aim of this work

The aim of this work is to simulate, for the first time to our knowledge, an entirely nonpolar peptide, a short-sequence peptaibol interacting with a lipid bilayer under conditions of low P/L. The primary goals are 1) to determine the mode of interaction of HZ with the bilayer by combination of the simulations with NMR experiments and 2) to establish the secondary structure on the basis of the simulations, also producing structural models for a subsequent solid-state NMR analysis. This will provide a comprehensive picture of the HZ molecule interacting with a DMPC bilayer at low P/L. In addition, free energies of the different possible orientations of HZ will be estimated. Also demonstrated will be any possible difficulties and challenges of application of MD simulation for such a system involving a nonpolar peptide, as opposed to applications to more usual polar or cationic peptides.

MATERIALS AND METHODS

Force fields, general simulation parameters, and starting structures

The molecular system to be simulated consisted of one HZ molecule of the sequence Ac-Aib-Asn-Ile-Ile-Aib-Pro-Leu-Leu-Aib-Pro-Leuol, a bilayer formed by 128 DMPC molecules, and ~ 3500 water molecules. The system was enclosed in a rectangular periodic box sized $\sim 6.3 \times 6.3 \times 6.0$ nm³. In the simulation with HZ starting outside the bilayer, the box size was increased by ~ 1 nm in the direction of the bilayer normal (z), and the number of water molecules was increased to 4300. A combination of the

following force fields was used to describe the system: Amber parm14SB (56–58) for the HZ molecule, slipids (59–61) for the DMPC molecules, and TIP3P (62) for the water.

All of the simulations were performed with the Gromacs package, versions 5.0.1 and 4.6.7 (63,64). The cumulative sampling in this study amounts to 32 μ s for the simulations presented in the main text (16 μ s of free simulations and 16 μ s of HREX), and 72 μ s for the additional simulations reported in the [Supporting Material](#) (8 μ s of HREX, 4 μ s of metadynamics, and 60 μ s of umbrella sampling). These are state-of-the-art timescales, approaching those in contemporary supercomputer studies of other authors like, e.g., that in Wang et al. (65).

Additional details can be referred to in the [Supporting Material](#).

Free MD simulations

A series of free MD simulations of HZ molecule interacting with the DMPC bilayer was performed, considering four different continuous initial conformations of the peptide: the α -helix, the 3_{10} -helix, the β -bend ribbon helix, and the fully extended conformation. Some simulations involved additional restraints to keep the conformation of HZ close to the initial one, as detailed in the [Supporting Material](#).

Restrained simulations were performed with three different initial conformations (which were also reference conformations for the restraints, at the same time): the α -helix, the 3_{10} -helix, and the β -bend ribbon. Unrestrained simulations were performed with two different initial conformations, the 3_{10} -helix and the fully extended conformation. For each of these five options regarding the conformation of HZ molecule, three different initial positions/orientations were considered: 1) HZ in the aqueous solvent, subject to heating-cooling protocol (see the [Supporting Material](#)) subsequently; 2) HZ inside the bilayer, with its molecular axis perpendicular to the bilayer surface; and 3) HZ inside the bilayer, immersed in the hydrophobic region, with the HZ axis parallel to the bilayer surface. Thus, in total 15 individual free MD simulations were performed, and every of them was extended to 1 μ s.

In addition, a cationic analog of HZ interacting with the DMPC bilayer was simulated. That peptide had an AA sequence Ace-Aib-Asn-Lys-Lys-Aib-Pro-Lys-Lys-Aib-Pro-Leuol and will be referred to as “HZ⁴⁺”. Its initial conformation was considered to be 3_{10} -helical, and the starting structure of the complete system was constructed with the heating-cooling protocol (see the [Supporting Material](#)). Then, an unrestrained MD simulation of 1 μ s was performed.

HREX

The replica-exchange method with solute tempering REST2 (66) was applied as implemented in Plumed 2.1.2 (67) interfaced to Gromacs 4.6.7. An HREX simulation was performed with eight replicas, in which the scaling factor λ followed a geometric series in the range of 1–0.3, corresponding to effective temperatures of 300–1000 K. The amplitudes of dihedrals in the HZ molecule were scaled by λ , and for the nonbonded interactions, the charges and Lennard-Jones depths of the atoms of HZ were scaled by $\sqrt{\lambda}$ and λ , respectively. The HREX simulation ran for 2 μ s, exchange was attempted every 2 ps for neighboring replicas, and the atomic coordinates were saved every 20 ps. The simulation was started with a 3_{10} -helical HZ molecule placed inside the DMPC bilayer, with its helical axis perpendicular to bilayer surface. No barostat was applied in the HREX simulations, thus an NVT canonical ensemble was sampled.

The trajectory generated by the unperturbed replica (scaling factor of one) was used to generate a plot of free energy as a function of two variables. These two collective variables were defined in the Cartesian coordinate system, with the DMPC bilayer oriented in the xy plane and the z axis being perpendicular to it, in the following way: The first variable was the distance in the z direction (i.e., projection of the distance on the z axis) between the center of mass (COM) of the HZ molecule and the COM of all

lipid atoms of the entire bilayer. The second variable was the angle between the major axis of the HZ molecule, and the z axis. To obtain the axis vector of HZ, the backbone atoms of HZ (all of the N, C α , C ω , and O atoms) were divided into two equally sized groups, one being N-terminal and the other being C-terminal, and a COM was obtained for each of them, $\vec{R}(N)$ and $\vec{R}(C)$. The helix axis was considered to pass through these two COMs, $\vec{R}(NC) = \vec{R}(C) - \vec{R}(N)$. Finally, the tilt angle was obtained from the z component of $\vec{R}(NC)$ as $\tau = \arccos(R_z(NC)/R(NC))$. The two-dimensional space in z and τ was divided into equally spaced bins of width of 0.20 Å and 1.1°, respectively, and the occurrences of (z, τ) from the replicas running with the unperturbed Hamiltonian were counted. The resulting probability distributions $\mathcal{P}(z, \tau)$ were recalculated to free energies as $\Delta G = -k_B T \log(\mathcal{P})$, with k_B being the Boltzmann constant and $T = 300$ K.

Experimental work

The description of the methodology can be referred to in the [Supporting Material](#).

RESULTS

Orientation of HZ from MD simulations

All-atom MD simulations were performed for one HZ molecule interacting with a DMPC bilayer. Fifteen independent trajectories over 1 μ s were generated, using different initial conformations, positions, and orientations of HZ in the bilayer. Some of the simulations employed distance or dihedral restraints to force a given secondary structure of the HZ molecule. The HZ molecule was always found embedded into the lipid bilayer in every simulation, and the dominant orientation observed in each of the simulations is presented in [Table 2](#).

A striking observation is that each of the many simulations started from different initial conditions converged to one of just two distinct structures. In what follows, these will be designated as the S-state—the HZ molecule is in the interfacial layer between the nonpolar and headgroup regions of the bilayer, with its main axis parallel to the bilayer

TABLE 2 Resulting Orientation of HZ in Each of the Individual Free MD Simulations Performed with the Different Initial Conditions

Initial Conformation	Restraints	In Solvent	Initial Position of HZ	
			In Bilayer: Initially Parallel	In Bilayer: Initially Perpendicular
α -helix	α	S	I	I
3_{10} -helix	3_{10}	I	I	I
β -bend ribbon	β -bend	I	I	I
Fully extended	none	S	S	I
3_{10} -helix	none	S*	S	I*

S, surface-bound orientation with HZ at the inner edge of the bilayer surface and the HZ axis parallel to the surface; I, transmembrane orientation with HZ axis perpendicular to the bilayer surface; the asterisks represent MD trajectories considered in the following analyses.

surface; and the I-state—the HZ molecule spans most of the hydrophobic bilayer width, with its main axis perpendicular to the bilayer surface. The representative instances of the S- and I-states are shown in Fig. 1.

It is also interesting that the outcome of MD simulations is different whenever the conformation of the HZ molecule is restrained to a certain structure by means of distance restraints imposed on H-bonds or backbone dihedral angles. Specifically, all of the simulations with HZ restrained to 3_{10} -helical or β -bend conformation actually led to an I-state orientation of HZ, no matter what the initial orientation in the simulation was. Thus, it seems that the flexibility of the HZ molecule may play a certain role in either the relative propensities of the different orientations or the process of insertion of HZ into the membrane.

All of the structural analyses below are based on the trajectories from two of the performed MD simulations, marked with asterisks in Table 2; these were unrestrained simulations with the HZ molecule in a 3_{10} -helical structure initially, placed either inside the bilayer perpendicular to its surface, which led to the I-state, or outside of the membrane and subjected to a heating-cooling protocol, which provided the S-state. Additionally, a simulation of a hypothetical charged mutant of HZ in an orientation resembling the S-state was performed. This molecule, HZ⁴⁺, has Ile³, Ile⁴, Leu⁷, and Leu⁸ replaced by lysines and carries four positive charges. To analyze the location of the peptide molecule within the bilayer in the different states in more detail, one-dimensional densities of atoms across the bilayer were obtained from MD trajectories (see Fig. 2). Also, the flexibility of conformation of the HZ molecule was quantified by means of the root-mean-squared fluctuation (see the Supporting Material); no noticeable features or differences between the I- and S-states were found.

I-State

The HZ molecule is oriented with its main axis along the bilayer normal direction, as reflected by the tilt angle fluctuating close to zero, of $22 \pm 13^\circ$ (mean \pm SD). The rather broad distribution may be due to the flexibility of the struc-

ture of the molecule, which affects the helical axis direction within the simple definition employed here. HZ spans the region of hydrophobic lipid tails symmetrically, and the displacement of the COM of HZ from the center of the bilayer is $0.0 \pm 1.7 \text{ \AA}$ (mean \pm SD). Thus, HZ is only slightly mobile along the direction perpendicular to the bilayer surface.

One of the striking properties of the HZ molecule is its small length, and a meaningful question to ask is if and how such a short molecule may span the entire width of a lipid bilayer. Notably, the considered DMPC bilayer is a rather thin one: its hydrophobic thickness of $\sim 25 \text{ \AA}$ in these simulations is well in the range of $23\text{--}27 \text{ \AA}$ found in the experimental literature (68–70). In the simplest idea of the peptide-bilayer interaction, the length of a hydrophobic peptide should match the hydrophobic thickness of the bilayer, to span the bilayer with no need for unfavorable interactions. To assess such a match, the length of the HZ molecule represented by the distance of the atoms C α of Aib¹ and Leu¹¹ was measured. With the length of $17.6 \pm 1.3 \text{ \AA}$, HZ is only slightly longer in the I-state than in the S-state ($16.3 \pm 1.3 \text{ \AA}$, mean \pm SD); the corresponding distributions are shown in the Supporting Material. Apparently, the HZ molecule is too short to match the hydrophobic region of even such a thin bilayer as DMPC when immersed in the I-state.

Still, the polar termini of HZ might reach into the head-group region of the bilayer if the bilayer is thinner in the vicinity of the HZ molecule; this would not be visible in the averaged density profiles in Fig. 2. To test this possibility, vertical density profiles were resolved by the horizontal distance from the COM of the HZ molecule (see Fig. 3). At distances above 15 \AA , the thickness of the hydrocarbon tail region of $24\text{--}25 \text{ \AA}$ corresponds to the unperturbed value. In the range of $5\text{--}10 \text{ \AA}$ from the HZ molecule, however, the observed thickness decreased locally to $\sim 20 \text{ \AA}$, and is similar in the range below 5 \AA . Thus, the hydrophobic region of the bilayer becomes thinner considerably in the vicinity of the HZ molecule. The termini of the HZ molecule in the I-state are capable of reaching into the lipid head-group region and may participate in favorable interactions

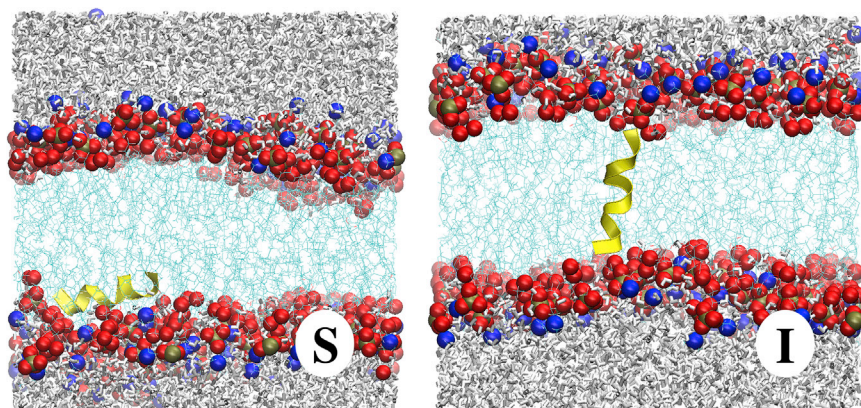


FIGURE 1 Given here are selected snapshots from free MD simulation, illustrating the two distinct orientations of the HZ molecule in a lipid bilayer that were observed: S-state (parallel to the surface, at its inner edge) and I-state (transmembrane, along the bilayer normal). To see this figure in color, go online.

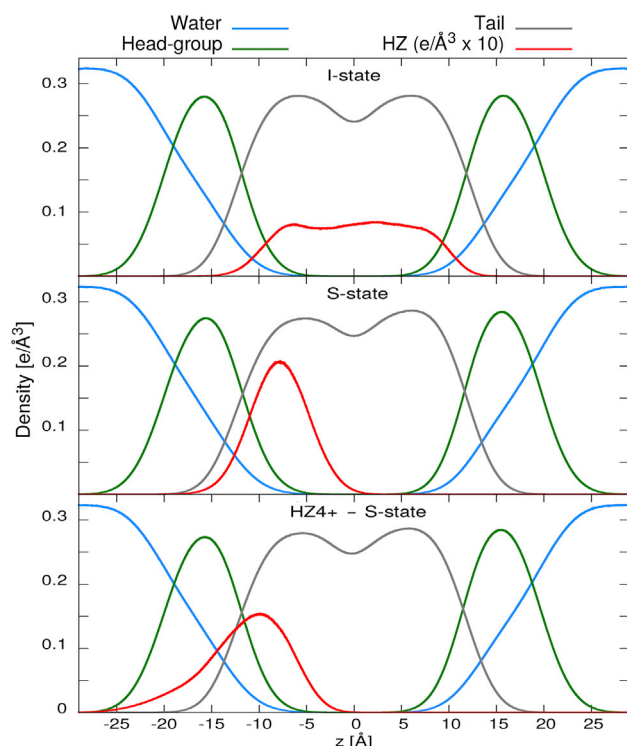


FIGURE 2 Given here are density profiles along the direction perpendicular to the bilayer plane, corresponding to the HZ molecule, water as well as the nonpolar tails and polar headgroups of the lipid. Electron density per unit volume ($e/\text{Å}^3$) is plotted for the I- and S-states of HZ as well as the S-state of the charged mutant HZ⁴⁺. To see this figure in color, go online.

like H-bonding. The local thickness of bilayer with an HZ molecule in the S-state is presented in the [Supporting Material](#) for comparison.

Previously, it was reported that a rather thick D(22:1)PC bilayer thinned with added ALM, the long-sequence peptaibol (71), and a POPC bilayer thinned considerably in the vicinity of an inserted molecule of the lipopeptaibol trichogin

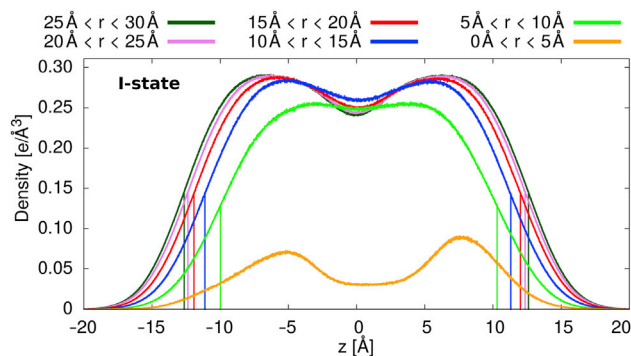


FIGURE 3 Given here are density profiles of the nonpolar hydrocarbon tails of DMPC in the simulation of HZ in the I-state. The different profiles were obtained considering lipid atoms in the given ranges of horizontal distances from the center-of-mass of the HZ molecule. (Horizontal distance is the distance projected in the plane of bilayer surface). To see this figure in color, go online.

GA IV (55). In this study, we have yet a different situation: there is a short-sequence peptaibol inserted into an inherently thin DMPC bilayer. Still, local thinning is observed, as an effort to reach a hydrophobic match of the inserted peptide and the hydrophobic thickness of the lipid bilayer.

S-State

A distinct observation is that the HZ molecule resides completely within the hydrophobic region of the bilayer, formed by the hydrophobic tails of the DMPC molecules. This is at odds with the usual behavior of amphiphilic membrane-active peptides, which often exhibit a strong interaction with the interface between the nonpolar and the polar regions due to the presence of one or more cationic amino acids (72). Such an effect is also observed in this study for the cationic mutant of HZ carrying four positive charges, HZ⁴⁺. Compared with HZ, HZ⁴⁺ is located much further from the center of the bilayer, roughly at the polar/nonpolar interface. This is reflected by the observed distance of HZ⁴⁺ from the center of the bilayer of $(11.5 \pm 2.7) \text{Å}$ being significantly larger than $(7.9 \pm 1.7) \text{Å}$ for the uncharged HZ (mean \pm SD). Let us rephrase this important observation: HZ is a strongly nonpolar peptide with no charged groups and few H-bonding donors or acceptors, and it is immersed nearly completely within the hydrophobic region of the bilayer, instead of interacting with the polar headgroups region in the way cationic peptides do.

Another structural feature of HZ is the orientation of the individual AA side chains, which describes the rotational state of HZ in the S-state along its helical axis. To this end, the z coordinate of the terminal heavy atom of each of the AA side chains (relative to the z coordinate of the COM of the HZ molecule) was calculated. These data, presented in Fig. 4, show which AA side chains point toward the hydrophobic volume preferentially, and which tend to interact with polar interface. Three of the five nonpolar side chains (Ile⁴, Leu⁷, and Leu⁸) point toward the

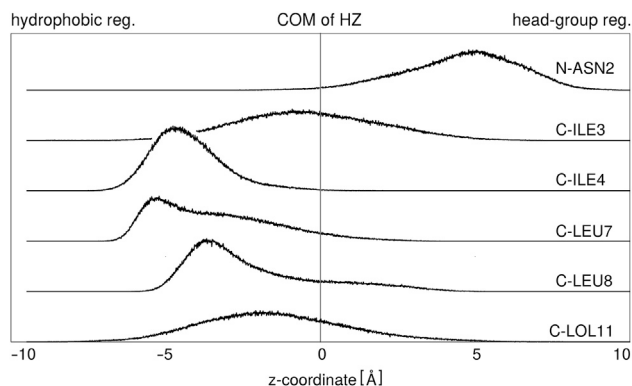


FIGURE 4 Shown here is the z coordinate of the terminal heavy atoms of the AA side chains except Aib and Pro. The value $z = 0$ corresponds to the center of mass of the HZ molecule; the side chain points toward the polar lipid headgroups if $z > 0$, whereas it points into the hydrophobic tail region if $z < 0$.

hydrophobic membrane region on average, and the two remaining ones (Leu¹¹ and Ile⁵) are rather indifferent. By contrast, the only polar side chain (Asn²) points clearly toward the headgroups of the lipid. Note that the system is dynamic, and it would be wrong to expect all of the AA side chains to assume the described orientation for 100% of the time. On the other hand, the clear shape of the distributions obtained from an MD trajectory of 1 μ s indicates that the result may be considered converged.

Experimental findings on the orientation of HZ in the bilayer

To provide experimental evidence in support of further MD analysis, we have performed biophysical characterization of the HZ in oriented zwitterionic bilayers and membrane mimics (unpublished data). We used ssNMR and synchrotron radiation circular dichroism (SRCD)—a combination of methods that is well established to experimentally characterize both overall conformation and orientation of α -helically folded membrane-active peptides (73–75). As can be seen in Fig. 5 A, HZ in 50% TFE (*black trace*) reveals CD spectrum with pronounced two negative bands at 205 nm (Band I) and \sim 220 nm (Band II) and a positive signal at \sim 190 nm. In general, this spectral shape corresponds to an overall helical fold but does not resemble continuous canonical secondary structure features of simple folds like α -helix, β -strand, random coil, poly-proline helix, etc. This appearance is closest to the spectra reported for 3_{10} -helically folded peptaibols and related model peptides composed of α -tetra-substituted amino acids (76,77), in that 1) Band I is shifted

to a lower wavelength than in an α -helix (205 nm instead of 208 nm) and 2) the Band I/Band II ratio is >1 . However, quantitative deconvolution of the SRCD data using the DICHROWEB server (78) and a 3_{10} -helix containing dataset (Set 2, data between 178–260 nm) (78,79) does not reveal any significant amount of 3_{10} -helix (8.4–10%, depending on the algorithm used). On the contrary, in these deconvolutions, α -helix and random coil fractions appear to prevail (with 28.6–35% and 29–34.7%, respectively). Although being impossible to quantitatively assess the amount of β -bend ribbon conformation—because there is no corresponding CD model available—this latter result suggests another possibility for the interpretation of the CD spectrum: HZ could be structured as a mixture of, e.g., α -helical/ 3_{10} -helix in the middle of the sequence, and a random coil/extended fold toward molecular termini.

The orientation of an α -helix in an OCD spectrum is easy to determine by analyzing the intensity at the fingerprint wavelength of 208 nm; in the used sample arrangement, positive ellipticities should indicate the I-state and negative values correspond to the S-state orientation (75). Because HZ is not folded as an α -helix, its Band I does not fit 208 nm, but the fact that irrespective of the bilayer composition, the spectral shape stays unchanged, and, besides, resembles the isotropic solution spectrum, allows us to suggest S-state alignment from the SROCD data. This result is further supported by ssNMR experiments (see Fig. 5 B). From the ^{31}P -NMR, a high degree of bilayer alignment ($>70\%$ lipid are oriented) is visible, and no significant bilayer disruption is seen for the HZ reconstituted at 1 mol %. Because the sample preparation for SROCD and

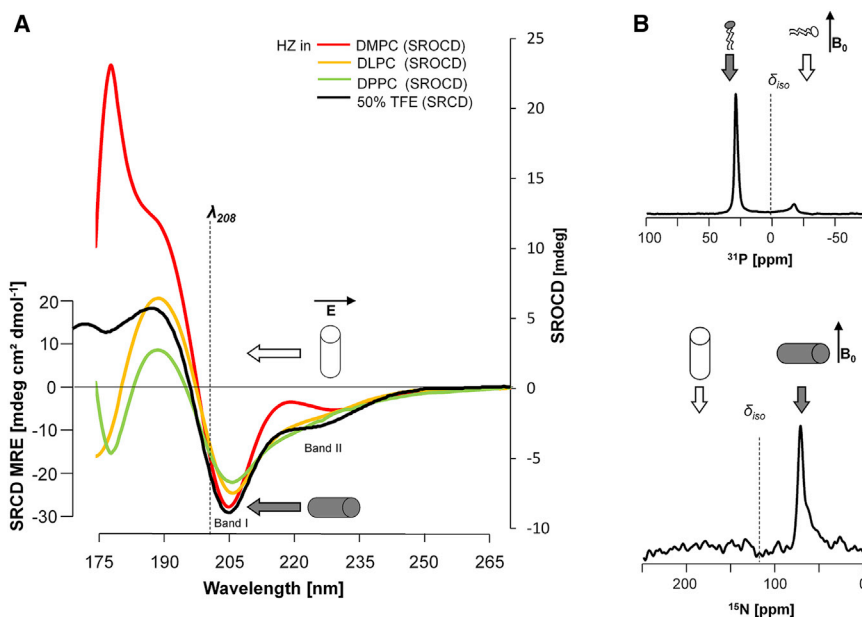


FIGURE 5 Experimental evaluation of the HZ orientation in phospholipid membranes. (A) Shown here are the SRCD (*black trace*, left ordinate) and SROCD (*colored traces*, right ordinate) spectra of HZ in isotropic solution (*black trace*) and oriented bilayers of DLPC, DMPC, and DPPC, each containing HZ at P/L of 1:100. Oriented samples are aligned with the bilayer normal (\vec{n}) parallel to the light propagation director. Dotted line ($\lambda = 208$ nm) depicts the wavelength that determines the alignment of α -helices in OCD: positive values correspond to the I-state alignment, whereas negative ellipticities suggest S-state or tilted alignment. Electric field vector (\vec{E}) and respective peptide (depicted as a *cylinder*) orientations are drawn schematically. Matched alignments (i.e., peptides being perpendicular to \vec{n}) are shown by the shaded filling. (B) Shown here are the solid-state ^{31}P -NMR (*top*) and ^{15}N -NMR (*bottom*) spectra of $\{^{15}\text{N}\}$ HZ reconstituted in oriented bilayers of DMPC at P/L 1:100. The sample is placed with \vec{n} parallel to external magnetic field \vec{B}_0 , and isotropic chemical shift frequencies are shown as dotted lines. Schematic drawings of a lipid (*top*), and a peptide, depicted as a cylinder (*bottom*), demonstrate alignments (i.e., lipids being parallel and peptides

being perpendicular to \vec{n} and \vec{B}_0) to which observed chemical shift anisotropy signal may correspond. Matched alignments (i.e., lipids being parallel and peptides being perpendicular to \vec{n} and \vec{B}_0) are shown by the shaded filling. To see this figure in color, go online.

ssNMR is nearly identical, a similar degree of membrane alignment is expected in CD samples. Moreover, in the ^{15}N -NMR spectra no powder signals could be detected, suggesting no aggregation of the peptide. The selectively labeled HZ demonstrates instead chemical shift of 98 ppm, a clearly coplanar orientation of the HN-COO vector localized in the middle of HZ sequence (at Leu⁷).

Taken together, SRCD and ssNMR data strongly suggest an S-state alignment of HZ in DMPC, but the conformational ambiguity is unresolved. The question of HZ structure remains to be answered either in a more detailed experimental study or by MD.

Structure of HZ from MD simulations

The structural ensembles of HZ were assessed. Besides the general goal, to characterize the conformation of the mole-

cule, a specific question was whether HZ assumes a β -bend ribbon (spiral), which can be considered a subclass of the 3_{10} -helical family. To this end, a structural analysis was performed for the MD trajectories of HZ inserted in the DMPC bilayer both in the S-state and the I-state. A Ramachandran plot was obtained separately for each of the AAs 3–10 in both MD trajectories (see Fig. 6), which also shows the averaged structures of HZ from the unrestrained simulations in the S- as well as I-states.

The distributions of (φ, ψ) of both Leu and of both Ile are rather broad, located in the helical region of the plot. There is also a certain overlap with the typical β -bend values; note here the large fluctuation of the values reported in Ségalas et al. (19), reprinted in Table 1. The (φ, ψ) distributions for Aib and Pro are more distinct, located along the line typical for 3_{10} -helices, and there is also a certain match with the β -bend for Pro and a modest one for Aib. In short, no clear

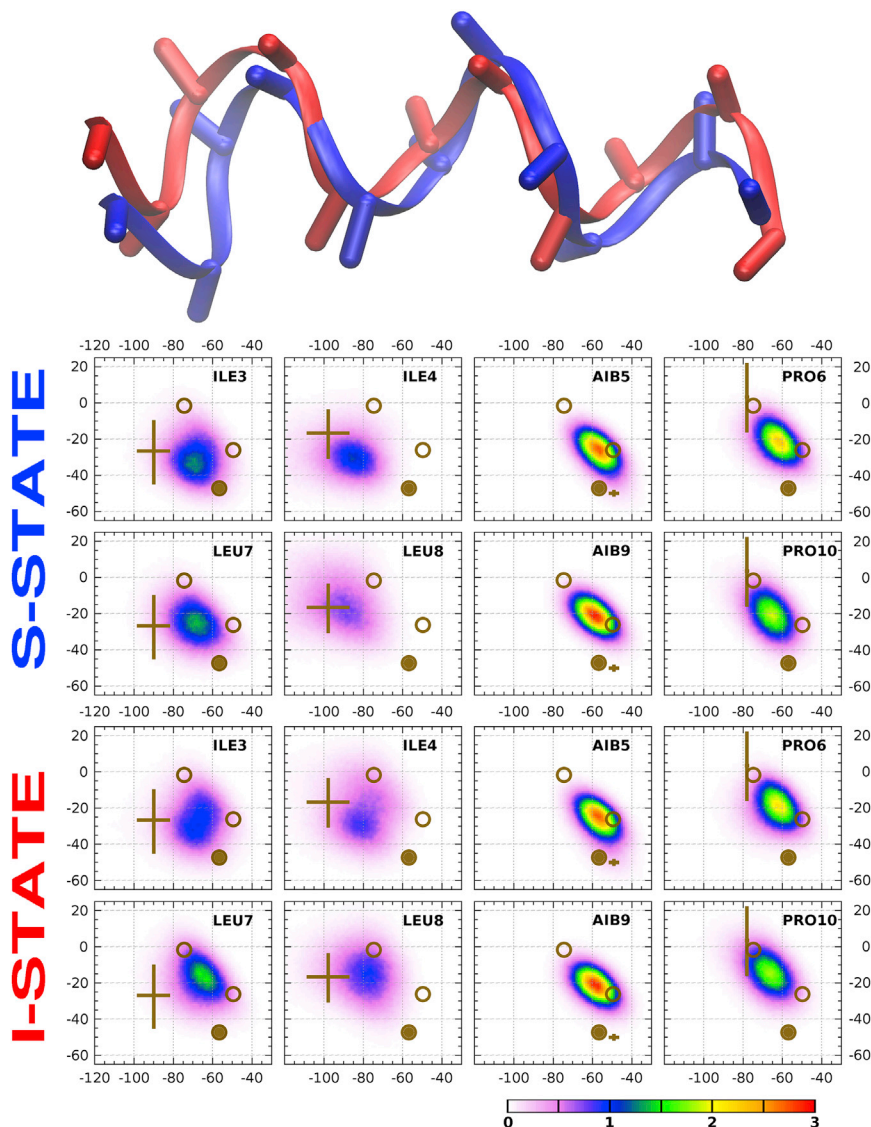


FIGURE 6 (Top) Given here are dominant conformations of the HZ molecule in the S-state (blue/dark) and the I-state (red/light). Structures were obtained with a PCA procedure run on MD trajectories, described in the Supporting Material. (Bottom) Given here are the Ramachandran plots for amino acids 3–10 of the HZ molecule interacting with a DMPC bilayer, in the S-state and in the I-state. The usual convention is employed (horizontal axis, φ and vertical axis, ψ , both in degrees); open circles, 3_{10} -helical conformations with $(-74^\circ, -4^\circ)$ and $(-49^\circ, -26^\circ)$; solid circles, α -helical conformation with $(-57^\circ, -47^\circ)$; the locations and sizes of crosses represent the ranges reported for the β -bend ribbons in Ségalas et al. (19). See the Supporting Material for numerical values of (φ, ψ) of the dominant conformations. To see this figure in color, go online.

conclusion on the conformation of HZ is possible based on the analysis of Ramachandran plots; it may only be stated that the conformations of HZ in the S- and I-states seem to be similar. The structures of HZ accumulated along the MD trajectories were also compared to static, idealized conformations by means of the root-mean-squared displacements of atomic positions (see the [Supporting Material](#)). The root-mean-squared displacement values with respect to β -bend ribbon as well as 3_{10} -helix are low, indicating a large similarity to the idealized structures, whereas α -helical conformation is less likely.

Just one conformational element that differs between HZ in the S- and I-states is apparent in the Ramachandran plots as well as visually in the averaged structures. The Ramachandran plots show ψ of Leu⁷ and ϕ of Leu⁸ to be shifted clearly if slightly, by $\sim 15^\circ$ (whereas ψ of Leu³ is shifted to an even lesser extent, by $\sim 10^\circ$). Accordingly, the average structures of HZ in the S- and I-states differ at the position 7–8. Apart from these particular features, few conformational distinctions are apparent.

Additional information on the structure of the HZ helix may be provided by the analysis of intrabackbone H-bonding patterns. To this end, lengths of putative backbone H-bonds typical of a 3_{10} -helical conformation were measured, and their distributions were obtained (see [Fig. 7 \(left\)](#)). Also here, there are very similar pictures of H-bonding for the HZ molecule in the S and I-states. Most

of the monitored putative H-bonds exhibit a distribution of length located close to 2 Å, showing good, stable H-bonding. However, two of the putative H-bonds, Asn² \leftarrow Aib⁵ and Pro⁶ \leftarrow Aib⁹, show distributions that are shifted to longer distances in the S-state, meaning that these H-bonds cease to exist over certain periods of the respective MD trajectory. A qualitative picture of H-bonding in the HZ molecule in the S- and I-states that follows is presented in [Fig. 7 \(right\)](#).

In the I-state, there is a continuous pattern of $i \leftarrow i + 3$ H-bonding along the entire HZ molecule, except the cases where a proline cannot be a hydrogen donor. By contrast, two more H-bonds are missing in HZ in the S-state: Asn² \leftarrow Aib⁵ and Pro⁶ \leftarrow Aib⁹. Strikingly, this observation correlates with the idea of two possible β -bends of the type Xaa-Yaa-Aib-Pro stretching over the residues Ile³–Pro⁶ and Leu⁷–Pro¹⁰. These two bends might constitute rather independent structural elements, with a flexible mutual arrangement. Thus, a β -bend ribbon conformation is possible for the HZ molecule in the S-state, whereas the conformation is rather 3_{10} -helical in the I-state.

The sampling of structural ensembles is a persistent issue in MD simulations of lipid bilayer systems. Therefore, a procedure based on the principal component analysis (PCA) was employed to examine the convergence in the MD trajectories of HZ in the S- and I-states. The results are detailed in the [Supporting Material](#). In a nutshell, the convergence of structural ensembles of HZ on the simulated timescale of 1 μ s was confirmed.

To summarize, the structure of HZ immersed in a DMPC bilayer was characterized. The interpretation shall concentrate on the structure in the S-state, which was revealed as the more likely orientation by the experimental study. The I-state, which may be an intermediate in, e.g., the oligomerization of HZ, shall also serve as a reference to accessible structural space. The Ramachandran analysis corroborated what a simple visual inspection indicated, namely that the molecule assumes a structure in the 3_{10} -helical family, and a tendency to form a β -bend ribbon was confirmed by the analysis of H-bonding. The Leu⁷–Leu⁸ segment was shown to be flexible: while it assumes a rather stretched conformation in the (less likely) I-state orientation, it is bent slightly in the dominant S-state orientation.

Free energies from replica exchange simulations

The HREX method was employed to determine the relative free energies of the different orientations of the HZ molecule in a DMPC bilayer. Within the HREX framework, the force-field contributions localized in the HZ molecule were scaled down in all but one of the eight replicas of the molecular complex. The starting structure in all replicas of the HREX simulation had the HZ molecule inside the bilayer, perpendicular to the bilayer plane, i.e., close to the I-state, and the HZ molecule remained within the bilayer

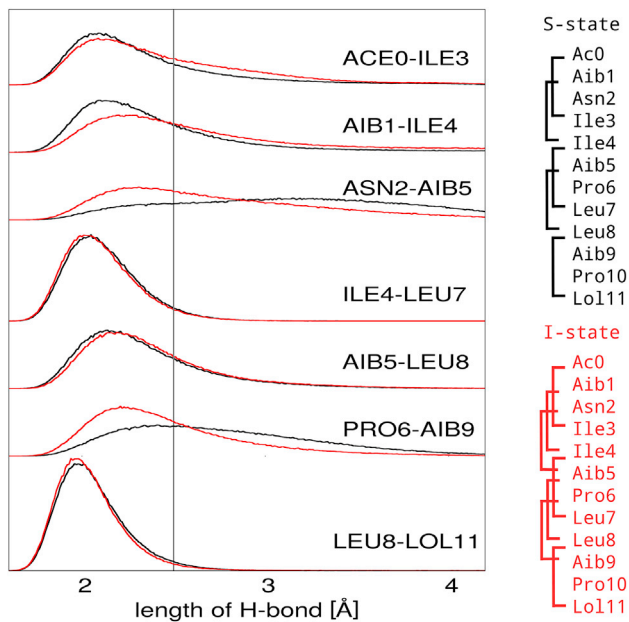


FIGURE 7 (Left) Shown here is the distribution of lengths of putative backbone hydrogen bonds in HZ, corresponding to the 3_{10} -helical conformation, in the S-state (black/dark) and in the I-state (red/light). ResX–ResY is the distance between the carboxy-O atom of ResX and the imino-H atom of ResY. The vertical line at 2.5 Å is a guide to the eye. (Right) Shown here are H-bonds present in the HZ molecule in the S and I-states. To see this figure in color, go online.

for the entire simulation time of $2 \mu\text{s}$. The resulting surface of free energy as a function of two variables—the z coordinate of the COM of HZ relative to the COM of bilayer, and the tilt angle between the long axis of HZ and the z axis—is presented in Fig. 8.

A pair of each of the two structures, the S- and I-states, observed in free simulations, are visible in the free energy plot clearly. Both of the S-states at $z \approx \pm 8 \text{ \AA}$ and tilt angle of $\sim 90^\circ$ are equally deep global minima of energy; they are set to zero free energy in Fig. 8. The I-states at $z = 0$ and tilt of 15° and 165° are secondary minima, which lie higher in energy than those corresponding to the S-states. Because both leaflets of the bilayer are equivalent, the I-state minima should be equally deep much like the S-state minima, therefore we consider this feature of the plot not converged. An achievement to be appreciated is that the global minima have been reproduced, and the secondary minima are present and higher in energy. Although this simulation of $2 \mu\text{s}$ already sampled several interconversions between the S- and I-states, an extension of the simulation would be necessary to have the secondary minima converged as well. A conclusion that may be made at this point is that both the S-state and the I-state have been confirmed as the relevant structures, with the S-state being the most likely structure, in accordance with the above experimental conclusion.

A technical point worth discussion is the efficiency of sampling with these HREX simulations. Recall that the difficult convergence is due to the very slow rearrangements of lipid hydrocarbon tails, leading to very slow equilibration in MD simulations. The idea of HREX is to reduce energy barriers by way of scaling down appropriate contributions to the force-field energy of the molecular system. Now, it is not obvious if the scaling of interactions involving a nonpolar molecule like HZ (with, prominently, nonpolar lipid components) may improve the rate of sampling or

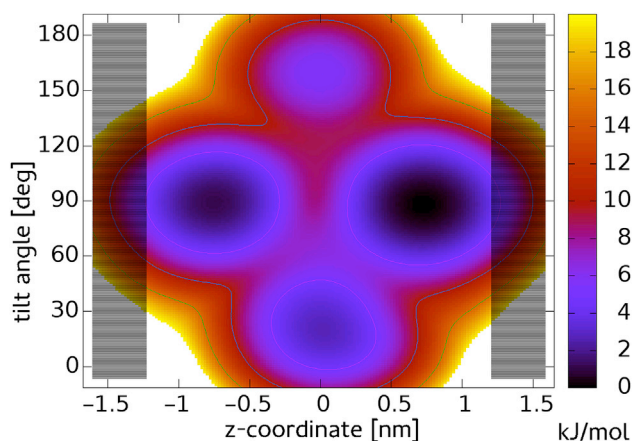


FIGURE 8 Given here is the free energy surface from the HREX simulation with an HZ molecule placed in the hydrocarbon tail region initially; shaded area indicates the region of polar lipid headgroups. To see this figure in color, go online.

not. A typical application of HREX would rely on the weakening of polar interactions or rotational barriers, which both do not apply in this study. This may be the reason for the failure of HREX to provide largely improved sampling efficiency.

An additional HREX simulation of $1 \mu\text{s}$ was performed with the HZ molecule placed in the aqueous phase initially, aiming at an estimate of the free energy profile of the HZ molecule passing from the solution to the bilayer (refer to the Supporting Material for a full report). There was, however, the problem that the HZ molecule only passed into the interior of the bilayer once, in a single HREX replica, during the microsecond simulation. Thus, it seems that obtaining convergence in such a simulation is far beyond the possibilities of current HREX methodology and computational equipment. The event of insertion that was observed may still constitute a starting point of a followup study of the mechanism of insertion. For the time being, we can merely state that the HZ molecule was inserted in the bilayer with its Leuol-terminus first (see Movie S1 in the Supporting Material). It has to be noted again that this event occurred once only, and took an amount of time that extended over several successful replica exchange instances; in other words, it took place in a simulation running with artificial and variant potential energy function.

DISCUSSION

We simulated a molecule of harzianin HK VI (HZ), a short-sequence peptaibol interacting with a DMPC bilayer. The goal was to assess the structure and orientation of HZ in the bilayer on the basis of unrestrained MD simulations. The simulations were complemented with ssNMR and SRCD experiments to facilitate a decision on the orientation. Further, it was attempted to estimate free energies from extended sampling simulations.

Two possible orientations of HZ in the bilayer were identified on the basis of free MD simulations: the I-state, with HZ perpendicular to the bilayer surface; and the S-state, where HZ lies in the hydrophobic part of the bilayer, close and parallel to its surface. The ensemble of simulations that were performed involved largely varying initial structures and orientations. Despite that, each of the simulations performed ended up in one of those two states. However, the sampling achieved in such free MD simulations was by far too insufficient to decide which of the orientations is preferred.

HREX simulations were performed to enhance the sampling of the different orientations of HZ in the bilayer. Even with this modern technique, however, it was still impossible to obtain a number of interconversions between the S- and I-states that would be sufficient to obtain conclusive results in terms of converged populations (or, equivalently, free energies). Calculation of free energies with extended metadynamics and umbrella sampling simulations

turned out to be even less practicable, as detailed in the [Supporting Material](#).

The issue of unclear dominant orientation was resolved by means of ssNMR and SRCD experiments. Their analysis revealed that the HZ molecule is embedded in the surface of the bilayer preferably, i.e., it assumes the S-state. On the other hand, it is conceivable that the I-state may act as an important, low-energy intermediate in the insertion into bilayer, transfer between the bilayer leaflets, or in a process of aggregation of HZ into oligomers at conditions of higher P/L. Therefore, the following analysis of structure addressed both the S- and the I-state.

The structure of HZ, for which no hard experimental evidence is available, was characterized on the basis of free MD simulations. These were converged with respect to HZ structure, as confirmed by an analysis based on PCA. Ramachandran plots were inspected, and intrabackbone H-bonding patterns were investigated. The conformation of the HZ molecule in both the S- and I-state orientations falls into the 3_{10} -helical family. Apparently, the HZ molecule is somewhat longer along the helical axis in the I-state than in the S-state. This goes to the account of the slightly different conformation of the Leu⁷-Leu⁸ moiety.

In the more relevant S-state, the HZ molecule is located completely within the hydrophobic region of the bilayer, in contrast to the behavior of cationic amphiphilic peptides that usually dock into the hydrophobic/hydrophilic interface. In other words, HZ is immersed deeper into the bilayer than an amphiphilic peptide of comparable size. In addition, the HZ molecule in the S-state assumes an oriented rotational state: the polar side chain of Asn² is pointing toward the headgroup region, whereas the nonpolar side chains—all of the others except both Aib side chains—are oriented into the interior of the bilayer.

In the I-state, the HZ molecule is too short to match the hydrophobic thickness of an unperturbed DMPC bilayer. However, our analysis of local thickness profiles revealed that the HZ molecule present in the I-state induces a local thinning of the DMPC bilayer. Then, the length of the HZ molecule closely matches the (decreased) thickness of the hydrophobic region of the bilayer in the immediate vicinity of HZ. Therefore, although the S-state is the dominant orientation, the I-state may represent a conceivable, viable intermediate in processes like insertion or oligomerization of HZ.

This study illustrated the grand challenge of simulation of nonpolar peptides in lipid bilayers. Extended sampling techniques proved to be of limited use: HREX simulations, and even more so biasing potential methods (metadynamics and umbrella sampling simulations) hardly produced any useful results despite the large computational effort taken. Note that extremely low efficiency of umbrella sampling simulations of AMP binding was reported in Neale et al. (80). A viable alternative may be an application of a coarse-grained force field, which would require the secondary

structure of HZ as an input for the parametrization. The results from this work could be used for this purpose, and we are currently working on an application for the oligomerization of HZ at elevated P/L.

SUPPORTING MATERIAL

Supporting Materials and Methods, Supporting Results, ten figures, one table, one movie, and one data file are available at [http://www.biophysj.org/biophysj/supplemental/S0006-3495\(17\)30558-1](http://www.biophysj.org/biophysj/supplemental/S0006-3495(17)30558-1).

AUTHOR CONTRIBUTIONS

S.A., S.L.G., T.B., A.S.U., and T.K. designed research. M.P. performed simulations. M.P., S.A., and T.K. analyzed simulations. S.K., A.B., G.C., and T.B. synthesized and purified the peptides. S.K. performed experiments with the help of S.A. and S.L.G. S.K., S.A., S.L.G., and A.S.U. analyzed experimental data. M.P., S.A., S.L.G., and T.K. wrote the article.

ACKNOWLEDGMENTS

This work was supported by the bwHPC Initiative and the bwHPC-C5 Project, funded by the state of Baden-Württemberg and the Research Foundation of Germany (DFG), through the services of the JUSTUS High Performance Computing Facility located at the University of Ulm, and further by the ANR-DFG grant 'Peptaibols' (DFG: UL 127/6-1), the Helmholtz Association program 'BIF-TM' and by the DFG (GRK 2039). We also acknowledge the ANKA CD-12 beamline as well as, personally, Jochen Bürck and Sigmar Roth.

SUPPORTING CITATIONS

References (81–96) appear in the [Supporting Material](#).

REFERENCES

- Leitgeb, B., A. Szekeres, ..., L. Kredics. 2007. The history of alamethicin: a review of the most extensively studied peptaibol. *Chem. Biodivers.* 4:1027–1051.
- Ruiz, N., G. Wielgosz-Collin, ..., Y. F. Pouchus. 2007. New trichobrachins, 11-residue peptaibols from a marine strain of *Trichoderma longibrachiatum*. *Peptides.* 28:1351–1358.
- Szekeres, A., B. Leitgeb, ..., C. Vágvölgyi. 2005. Peptaibols and related peptaibiotics of *Trichoderma*. A review. *Acta Microbiol. Immunol. Hung.* 52:137–168.
- Banerjee, R., S. Chattopadhyay, and G. Basu. 2009. Conformational preferences of a short Aib/Ala-based water-soluble peptide as a function of temperature. *Proteins.* 76:184–200.
- Grubišić, S., B. Chandramouli, ..., G. Brancato. 2016. Chain length, temperature and solvent effects on the structural properties of α -aminoisobutyric acid homooligopeptides. *Phys. Chem. Chem. Phys.* 18: 20389–20398.
- Ueda, A., M. Oba, ..., M. Tanaka. 2016. Helical structures of homochiral isotope-labeled α -aminoisobutyric acid peptides. *Tetrahedron.* 72:5864–5871.
- Meyer, C. E., and F. Reusser. 1967. A polypeptide antibacterial agent isolated from *Trichoderma viride*. *Experientia.* 23:85–86.
- Fox, R. O., Jr., and F. M. Richards. 1982. A voltage-gated ion channel model inferred from the crystal structure of alamethicin at 1.5-Å resolution. *Nature.* 300:325–330.

9. Mathew, M. K., and P. Balaram. 1983. A helix dipole model for alamethicin and related transmembrane channels. *FEBS Lett.* 157:1–5.
10. Wada, S., A. Iida, ..., T. Fujita. 1996. Ion channel-forming property of trichorovin-XII, an 11-residue peptaibol from the fungus *Trichoderma viride*, in planar lipid bilayer membranes. *Bioorg. Med. Chem. Lett.* 6:2275–2278.
11. Mazzuca, C., L. Stella, ..., B. Pispisa. 2005. Mechanism of membrane activity of the antibiotic trichogin GA IV: a two-state transition controlled by peptide concentration. *Biophys. J.* 88:3411–3421.
12. Rebuffat, S., S. Hlimi, ..., B. Bodo. 1996. Isolation and structural elucidation of the 11-residue peptaibol antibiotic, harzianin HK VI. *J. Chem. Soc., Perkin Trans. 1.* 2021–2027.
13. Poirier, L., F. Quiniou, ..., Y. F. Pouchus. 2007. Toxicity assessment of peptaibols and contaminated sediments on *Crassostrea gigas* embryos. *Aquat. Toxicol.* 83:254–262.
14. Antal, Z., L. Kredics, ..., E. Nagy. 2005. Comparative study of potential virulence factors in human pathogenic and saprophytic *Trichoderma longibrachiatum* strains. *Acta Microbiol. Immunol. Hung.* 52:341–350.
15. Mikkola, R., M. A. Andersson, ..., M. S. Salkinoja-Salonen. 2012. 20-Residue and 11-residue peptaibols from the fungus *Trichoderma longibrachiatum* are synergistic in forming Na⁺/K⁺-permeable channels and adverse action towards mammalian cells. *FEBS J.* 279:4172–4190.
16. Wada, S. I., and R. Tanaka. 2004. A novel 11-residual peptaibol-derived carrier peptide for in vitro oligodeoxynucleotide delivery into cell. *Bioorg. Med. Chem. Lett.* 14:2563–2566.
17. Wada, S., Y. Hitora, ..., H. Urata. 2012. Cellular uptake of covalent conjugates of oligonucleotide with membrane-modifying peptide, peptaibol. *Bioorg. Med. Chem.* 20:3219–3222.
18. Schirmböck, M., M. Lorito, ..., C. P. Kubicek. 1994. Parallel formation and synergism of hydrolytic enzymes and peptaibol antibiotics, molecular mechanisms involved in the antagonistic action of *Trichoderma harzianum* against phytopathogenic fungi. *Appl. Environ. Microbiol.* 60:4364–4370.
19. Ségalas, I., Y. Prigent, ..., S. Rebuffat. 1999. Characterization of a type of β -bend ribbon spiral generated by the repeating (Xaa-Yaa-Aib-Pro) motif: the solution structure of harzianin HC IX, a 14-residue peptaibol forming voltage-dependent ion channels. *Biopolymers.* 50:71–85.
20. Kandt, C., W. L. Ash, and D. P. Tieleman. 2007. Setting up and running molecular dynamics simulations of membrane proteins. *Methods.* 41:475–488.
21. Lindahl, E., and M. S. P. Sansom. 2008. Membrane proteins: molecular dynamics simulations. *Curr. Opin. Struct. Biol.* 18:425–431.
22. Feller, S. 2001. *Molecular Dynamics Simulation of Phospholipid Bilayers.* Springer, Berlin, Germany, pp. 89–107.
23. Berendsen, H. J. C., and D. P. Tieleman. 2002. *Molecular Dynamics: Studies of Lipid Bilayers.* John Wiley & Sons, Hoboken, NJ.
24. Lyubartsev, A. P., and A. L. Rabinovich. 2016. Force field development for lipid membrane simulations. *Biochim. Biophys. Acta.* 1858:2483–2497.
25. Chipot, C., and A. Pohorille. 1997. Structure and dynamics of small peptides at aqueous interfaces: a multi-nanosecond molecular dynamics study. *J. Mol. Struct. THEOCHEM.* 398–399:529–535.
26. Chipot, C., and A. Pohorille. 1998. Folding and translocation of the undecamer of poly-L-leucine across the water-hexane interface. A molecular dynamics study. *J. Am. Chem. Soc.* 120:11912–11924.
27. Tieleman, D. P., H. J. C. Berendsen, and M. S. P. Sansom. 1999. Surface binding of alamethicin stabilizes its helical structure: molecular dynamics simulations. *Biophys. J.* 76:3186–3191.
28. Alecio, M. R., D. E. Golan, ..., R. R. Rando. 1982. Use of a fluorescent cholesterol derivative to measure lateral mobility of cholesterol in membranes. *Proc. Natl. Acad. Sci. USA.* 79:5171–5174.
29. Tamm, L. K., and H. M. McConnell. 1985. Supported phospholipid bilayers. *Biophys. J.* 47:105–113.
30. Mills, R. 1973. Self-diffusion in normal and heavy water in the range 1–45°. *J. Phys. Chem.* 77:685–688.
31. Bond, P. J., J. Holyoake, ..., M. S. P. Sansom. 2007. Coarse-grained molecular dynamics simulations of membrane proteins and peptides. *J. Struct. Biol.* 157:593–605.
32. Monticelli, L., S. K. Kandasamy, ..., S.-J. Marrink. 2008. The MARTINI coarse-grained force field: extension to proteins. *J. Chem. Theory Comput.* 4:819–834.
33. Rzepiela, A. J., D. Sengupta, ..., S.-J. Marrink. 2010. Membrane poration by antimicrobial peptides combining atomistic and coarse-grained descriptions. *Faraday Discuss.* 144:431–443, discussion 445–481.
34. Parton, D. L., E. V. Akhmatkaya, and M. S. P. Sansom. 2012. Multi-scale simulations of the antimicrobial peptide maculatin 1.1: water permeation through disordered aggregates. *J. Phys. Chem. B.* 116: 8485–8493.
35. Horn, J. N., T. D. Romo, and A. Grossfield. 2013. Simulating the mechanism of antimicrobial lipopeptides with all-atom molecular dynamics. *Biochemistry.* 52:5604–5610.
36. Lin, D., and A. Grossfield. 2014. Thermodynamics of antimicrobial lipopeptide binding to membranes: origins of affinity and selectivity. *Biophys. J.* 107:1862–1872.
37. Wang, Y., T. Zhao, ..., J. P. Ulmschneider. 2014. How reliable are molecular dynamics simulations of membrane active antimicrobial peptides? *Biochim. Biophys. Acta.* 1838:2280–2288.
38. Gurtovenko, A. A., J. Anwar, and I. Vattulainen. 2010. Defect-mediated trafficking across cell membranes: insights from in silico modeling. *Chem. Rev.* 110:6077–6103.
39. Hub, J. S., B. L. de Groot, ..., G. Groenhof. 2014. Quantifying artifacts in Ewald simulations of inhomogeneous systems with a net charge. *J. Chem. Theory Comput.* 10:381–390.
40. Sugita, Y., and Y. Okamoto. 1999. Replica-exchange molecular dynamics method for protein folding. *Chem. Phys. Lett.* 314:141–151.
41. Im, W., and C. L. Brooks, 3rd. 2005. Interfacial folding and membrane insertion of designed peptides studied by molecular dynamics simulations. *Proc. Natl. Acad. Sci. USA.* 102:6771–6776.
42. Nymeyer, H., T. B. Woolf, and A. E. Garcia. 2005. Folding is not required for bilayer insertion: replica exchange simulations of an α -helical peptide with an explicit lipid bilayer. *Proteins.* 59:783–790.
43. Vogel, A., M. Roark, and S. E. Feller. 2012. A reinterpretation of neutron scattering experiments on a lipidated Ras peptide using replica exchange molecular dynamics. *Biochim. Biophys. Acta.* 1818:219–224.
44. Li, J., R. Lakshminarayanan, ..., R. W. Beuerman. 2012. Molecular dynamics simulations of a new branched antimicrobial peptide: a comparison of force fields. *J. Chem. Phys.* 137:215101.
45. Groot, R. D., and K. L. Rabone. 2001. Mesoscopic simulation of cell membrane damage, morphology change and rupture by nonionic surfactants. *Biophys. J.* 81:725–736.
46. Chen, L., N. Jia, ..., L. Golubovic. 2013. Effects of antimicrobial peptide revealed by simulations: translocation, pore formation, membrane corrugation and Euler buckling. *Int. J. Mol. Sci.* 14:7932–7958.
47. Lin, D., and A. Grossfield. 2015. Thermodynamics of micelle formation and membrane fusion modulate antimicrobial lipopeptide activity. *Biophys. J.* 109:750–759.
48. Bereau, T., W. F. D. Bennett, ..., M. Karttunen. 2015. Folding and insertion thermodynamics of the transmembrane WALP peptide. *J. Chem. Phys.* 143:243127.
49. Tieleman, D. P., M. S. P. Sansom, and H. J. C. Berendsen. 1999. Alamethicin helices in a bilayer and in solution: molecular dynamics simulations. *Biophys. J.* 76:40–49.
50. Tieleman, D. P., H. J. C. Berendsen, and M. S. P. Sansom. 2001. Voltage-dependent insertion of alamethicin at phospholipid/water and octane/water interfaces. *Biophys. J.* 80:331–346.
51. Tieleman, D. P., B. Hess, and M. S. P. Sansom. 2002. Analysis and evaluation of channel models: simulations of alamethicin. *Biophys. J.* 83:2393–2407.
52. Thøgersen, L., B. Schjøtt, ..., E. Tajkhorshid. 2008. Peptide aggregation and pore formation in a lipid bilayer: a combined coarse-grained and all atom molecular dynamics study. *Biophys. J.* 95:4337–4347.

53. Násztor, Z., J. Horváth, and B. Leitgeb. 2013. Structural characterization of the short peptaibols trichobranchins by molecular-dynamics methods. *Chem. Biodivers.* 10:876–886.
54. Násztor, Z., J. Horváth, and B. Leitgeb. 2015. In silico conformational analysis of the short-sequence hypomurocin A peptides. *Int. J. Pept.* 2015:281065.
55. Bobone, S., Y. Gerelli, ..., L. Stella. 2013. Membrane thickness and the mechanism of action of the short peptaibol trichogin GA IV. *Biochim. Biophys. Acta.* 1828:1013–1024.
56. Hornak, V., R. Abel, ..., C. Simmerling. 2006. Comparison of multiple Amber force fields and development of improved protein backbone parameters. *Proteins.* 65:712–725.
57. Wickstrom, L., A. Okur, and C. Simmerling. 2009. Evaluating the performance of the ff99SB force field based on NMR scalar coupling data. *Biophys. J.* 97:853–856.
58. Maier, J. A., C. Martinez, ..., C. Simmerling. 2015. ff14SB: improving the accuracy of protein side chain and backbone parameters from ff99SB. *J. Chem. Theory Comput.* 11:3696–3713.
59. Jämbeck, J. P. M., and A. P. Lyubartsev. 2012. Derivation and systematic validation of a refined all-atom force field for phosphatidylcholine lipids. *J. Phys. Chem. B.* 116:3164–3179.
60. Jämbeck, J. P. M., and A. P. Lyubartsev. 2012. An extension and further validation of an all-atomistic force field for biological membranes. *J. Chem. Theory Comput.* 8:2938–2948.
61. Jämbeck, J. P. M., and A. P. Lyubartsev. 2013. Another piece of the membrane puzzle: extending lipids further. *J. Chem. Theory Comput.* 9:774–784.
62. Jorgensen, W. L., J. Chandrasekhar, ..., M. L. Klein. 1983. Comparison of simple potential functions for simulating liquid water. *J. Chem. Phys.* 79:926–935.
63. Berendsen, H. J. C., D. van der Spoel, and R. van Drunen. 1995. GROMACS: a message-passing parallel molecular dynamics implementation. *Comput. Phys. Commun.* 91:43–56.
64. Abraham, M. J., T. Murtola, ..., E. Lindahl. 2015. GROMACS: high performance molecular simulations through multi-level parallelism from laptops to supercomputers. *SoftwareX.* 1–2:19–25.
65. Wang, Y., C. H. Chen, ..., J. P. Ulmschneider. 2016. Spontaneous formation of structurally diverse membrane channel architectures from a single antimicrobial peptide. *Nat. Commun.* 7:13535.
66. Wang, L., R. A. Friesner, and B. J. Berne. 2011. Replica exchange with solute scaling: a more efficient version of replica exchange with solute tempering (REST2). *J. Phys. Chem. B.* 115:9431–9438.
67. Tribello, G. A., M. Bonomi, ..., G. Bussi. 2014. PLUMED 2: new feathers for an old bird. *Comput. Phys. Commun.* 185:604–613.
68. Lewis, B. A., and D. M. Engelman. 1983. Lipid bilayer thickness varies linearly with acyl chain length in fluid phosphatidylcholine vesicles. *J. Mol. Biol.* 166:211–217.
69. Balgavý, P., M. Dubničková, ..., D. Uhríková. 2001. Bilayer thickness and lipid interface area in unilamellar extruded 1,2-diacylphosphatidylcholine liposomes: a small-angle neutron scattering study. *Biochim. Biophys. Acta. Biomembr.* 1512:40–52.
70. Kučerka, N., Y. Liu, ..., J. F. Nagle. 2005. Structure of fully hydrated fluid phase DMPC and DLPC lipid bilayers using x-ray scattering from oriented multilamellar arrays and from unilamellar vesicles. *Biophys. J.* 88:2626–2637.
71. Pan, J., D. P. Tieleman, ..., S. Tristram-Nagle. 2009. Alamethicin in lipid bilayers: combined use of x-ray scattering and MD simulations. *Biochim. Biophys. Acta. Biomembr.* 1788:1387–1397.
72. Hong, M., and Y. Su. 2011. Structure and dynamics of cationic membrane peptides and proteins: insights from solid-state NMR. *Protein Sci.* 20:641–655.
73. Grage, S. L., S. Afonin, and A. S. Ulrich. 2010. Dynamic transitions of membrane-active peptides. *Methods Mol. Biol.* 618:183–207.
74. Wallace, B. A., and R. W. Janes. 2010. Synchrotron radiation circular dichroism (SRCD) spectroscopy: an enhanced method for examining protein conformations and protein interactions. *Biochem. Soc. Trans.* 38:861–873.
75. Bürck, J., P. Wadhvani, ..., A. S. Ulrich. 2016. Oriented circular dichroism: a method to characterize membrane-active peptides in oriented lipid bilayers. *Acc. Chem. Res.* 49:184–192.
76. Toniolo, C., A. Polese, ..., J. Kamphuis. 1996. Circular dichroism spectrum of a peptide 3_{10} -helix. *J. Am. Chem. Soc.* 118:2744–2745.
77. Formaggio, F., C. Peggion, ..., C. Toniolo. 2004. Recent contributions of electronic circular dichroism to the investigation of oligopeptide conformations. *Chirality.* 16:388–397.
78. Whitmore, L., and B. A. Wallace. 2008. Protein secondary structure analyses from circular dichroism spectroscopy: methods and reference databases. *Biopolymers.* 89:392–400.
79. Janes, R. W. 2009. Reference datasets for protein circular dichroism and synchrotron radiation circular dichroism spectroscopic analyses. In *Advances in Biomedical Spectroscopy, I.* IOS Press, Amsterdam, the Netherlands, pp. 183–201.
80. Neale, C., J. C. Hsu, ..., R. Pomès. 2014. Indolicidin binding induces thinning of a lipid bilayer. *Biophys. J.* 106:L29–L31.
81. Bürck, J., S. Roth, ..., A. S. Ulrich. 2015. UV-CD12: synchrotron radiation circular dichroism beamline at ANKA. *J. Synchrotron Radiat.* 22:844–852.
82. Bayly, C. I., P. Cieplak, ..., P. A. Kollman. 1993. A well-behaved electrostatic potential based method using charge restraints for deriving atomic charges: the RESP model. *J. Phys. Chem.* 97:10269–10280.
83. Frisch, M. J., G. W. Trucks, ..., D. J. Fox. 2009. Gaussian 09 Revision C.01. Gaussian, Wallingford CT.
84. Darden, T., D. York, and L. Pedersen. 1993. Particle mesh Ewald—an $n \cdot \log(n)$ method for Ewald sums in large systems. *J. Chem. Phys.* 98:10089–10092.
85. Gromacs. 2016. *Gromacs Reference Manual, version 2016, section 4.9.1.* <http://manual.gromacs.org/documentation/2016/manual-2016.pdf>, last accessed 7 Sep 2016.
86. Hess, B., H. Bekker, ..., J. G. E. M. Fraaije. 1997. LINCS: a linear constraint solver for molecular simulations. *J. Comput. Chem.* 18:1463–1472.
87. Nosé, S. 1984. A molecular dynamics method for simulations in the canonical ensemble. *Mol. Phys.* 52:255–268.
88. Hoover, W. G. 1985. Canonical dynamics: equilibrium phase-space distributions. *Phys. Rev. A.* 31:1695–1697.
89. Nosé, S., and M. L. Klein. 1983. Constant pressure molecular dynamics for molecular systems. *Mol. Phys.* 50:1055–1076.
90. Ulmschneider, J. P., J. C. Smith, ..., E. Strandberg. 2012. Reorientation and dimerization of the membrane-bound antimicrobial peptide PGLa from microsecond all-atom MD simulations. *Biophys. J.* 103:472–482.
91. AmberTools. 2010. *Amber Tools 1.4.* <http://ambermd.org>.
92. Laio, A., and M. Parrinello. 2002. Escaping free-energy minima. *Proc. Natl. Acad. Sci. USA.* 99:12562–12566.
93. Barducci, A., G. Bussi, and M. Parrinello. 2008. Well-tempered metadynamics: a smoothly converging and tunable free-energy method. *Phys. Rev. Lett.* 100:020603.
94. Jämbeck, J. P. M., and A. P. Lyubartsev. 2013. Exploring the free energy landscape of solutes embedded in lipid bilayers. *J. Phys. Chem. Lett.* 4:1781–1787.
95. Bochicchio, D., E. Panizon, ..., G. Rossi. 2015. Calculating the free energy of transfer of small solutes into a model lipid membrane: comparison between metadynamics and umbrella sampling. *J. Chem. Phys.* 143:144108.
96. Filipe, H. A. L., M. J. Moreno, ..., L. M. S. Loura. 2014. How to tackle the issues in free energy simulations of long amphiphiles interacting with lipid membranes: convergence and local membrane deformations. *J. Phys. Chem. B.* 118:3572–3581.

Biophysical Journal, Volume 112

Supplemental Information

**Structural Behavior of the Peptaibol Harzianin HK VI in a DMPC Bilayer:
Insights from MD Simulations**

**Marina Putzu, Sezgin Kara, Sergii Afonin, Stephan L. Grage, Andrea Bordessa, Grégory
Chaume, Thierry Brigaud, Anne S. Ulrich, and Tomáš Kubař**

I. METHODS

A. Force field, general simulation parameters, and starting structures

The needed sets of atomic charges for the non-standard residues Aib and Leuol were obtained by restrained electric potential fitting method (RESP)¹ with molecular electric potentials obtained on the HF/6-31G* level of theory, and the parameters for torsions along the backbone dihedral angles of Aib were obtained by fitting to data generated on the B3LYP/TZVP level. Quantum chemical calculations were performed with Gaussian 09,² and the parameter and topology files for Aib and Leuol are attached to this Supporting Information as a zip archive (`Amber_files.zip`). Long-range electrostatic interactions were treated with the particle-mesh Ewald scheme (PME),³ using a real-space cutoff of 1.0 nm, Fourier spacing of 0.12 nm and a fourth-order interpolation to the Ewald mesh. Van der Waals interactions were cut off at 1.0 nm. Long-range dispersion correction to the pressure and potential energy were considered.⁴

The leap-frog integrator was applied with a time step of 2 fs, and all of the covalent bonds were constrained by means of the LINCS algorithm.⁵ All production simulations were performed in the NPT ensemble, where the temperature was kept constant with the Nosé-Hoover thermostat,^{6,7} with solvent, peptide and lipid coupled to separate heat baths with coupling constants of 0.5 ps. The pressure was maintained constant with a semi-isotropic scheme, so that the pressure in the membrane plane was controlled separately from the pressure in the membrane normal direction, and the Parrinello-Rahman barostat⁸ was applied with a reference pressure of 1 bar, a coupling constant of 2 ps, and a compressibility of $4.5 \times 10^{-5} \text{ bar}^{-1}$. The coordinates of atoms were saved every 2 ps.

To build the structure of the system, use was made of a DMPC bilayer containing 128 molecules (64 per leaflet) pre-equilibrated at 303 K, which was downloaded from the Slipids web site.⁹ Two different protocols were employed to create the initial structures of the HZ-bilayer system: (i) The HZ molecule was placed in the aqueous phase and the pre-equilibrated DMPC bilayer was left intact. First, 5 ns of MD simulation were performed at 480 K, which led to the insertion of HZ into the bilayer within 2 ns. Then, the system was cooled down with further 40 ns of simulation with a reference temperature of 300 K. This procedure will be referred to as the heating-cooling protocol.¹⁰ (ii) The structure of the HZ

molecule immersed in the DMPC bilayer was generated directly with Inflategro,¹¹ and an equilibration simulation of 40 ns was performed.

B. Free MD simulation

The initial structures of HZ were constructed with the xLeap program of the AmberTools package,¹² and the initial backbone dihedral angles applied are shown in Tab. I.

Conformation	Residue	φ	ψ	ω
α -helix		-60°	-45°	180°
3_{10} -helix		-50°	-25°	180°
β -bend	Xaa1	-90°	-27°	180°
	Yaa2	-98°	-17°	180°
	Aib3	-49°	-50°	180°
	Pro4	-78°	$+3^\circ$	180°
extended		180°	180°	180°

TABLE I. Idealized backbone dihedral angles of the considered initial conformations of the HZ molecule. The values for the β -bend ribbon spiral taken from Ref. 13.

Some simulations involved additional restraints in order to keep the conformation of HZ close to the initial one. For the helical conformations, 3_{10} and α , these took the form of harmonic distance restraints on all of the backbone hydrogen bonds, $V(d) = \frac{1}{2}k(d - d_0)^2$ with d being the length of the hydrogen bond, and the parameters $k = 50 \text{ kJ mol}^{-1} \text{ \AA}^{-2}$ and $d_0 = 2.4 \text{ \AA}$. The two prolines in the HZ molecule cannot act as hydrogen donors, and in these cases, the restraints were applied to the distance b between the unsatisfied hydrogen acceptor (the amido oxygen atom of the amino acid three or four residues upstream, for 3_{10} and α , respectively) and the nitrogen of the proline, with $b = 4.0 \text{ \AA}$. For the β -bend ribbon structure, harmonic restraints of the form $V(\zeta) = \frac{1}{2}k(\zeta - \zeta_0)^2$ were applied on the backbone dihedral angles of the two motifs Xaa–Yaa–Aib–Pro, i.e., amino acid residues 3–10, with $k = 1.523 \text{ kJ mol}^{-1} \text{ deg}^{-2}$.

C. Experimental work

Peptide synthesis/purification. Two HZ peptides – a native sequence and the ^{15}N -labelled version ($\{^{15}\text{N}\}\text{HZ}$, Ac-Aib-Asn-Ile-Ile-Aib-Pro- $\{^{15}\text{N}\}$ Leu-Leu-Aib-Pro-Leuol) for solid-state NMR – were synthesized using automated solid-phase peptide synthesis on a Liberty Blue CEM instrument. The synthesis was performed starting from H-L-leucinol-2-chlorotrityl resin. Fmoc strategy protocols were used and each amino acid was coupled two times. Diisopropylcarbodiimide/OxymaPur was employed as a coupling reagent. Coupling reactions for all amino acids were accomplished under conditions of microwave activation for 2 min at 90 °C except for the Fmoc-Aib-OH (at 50 °C for 10 min). Fmoc deprotections were carried out one time using 20% piperidine for 3 min at 75 °C, except for the Fmoc-Aib-OH (2×10 min at 25 °C). N-terminal acetylation of the peptidyl resins was performed manually by a double treatment with acetic anhydride and N-methylmorpholine for 1 h at ambient temperature. The 1,2-aminoalcohol peptides were cleaved from the resin upon 4 treatments with the hexafluoro-2-propanol/dichloromethane (1:4, vol) mixture for 1 h. The crude peptides were purified ($> 98\%$ purity) by semi-preparative reverse phase (C18) high-performance liquid chromatography (HPLC) and characterized by reverse phase (C18) HPLC-mass spectrometry (ESI) and by analytical reverse phase (C18) HPLC, each time using gradient elution with water/acetonitrile mixtures supplemented with 0.1 % TFA as the ion-pairing agent.

Lipids. Saturated lipids – 1,2-dilauroyl-*sn*-glycero-3-phosphocholine (DLPC), 1,2-dimyristoyl-*sn*-glycero-3-phosphocholine (DMPC) and 1,2-dipalmitoyl-*sn*-glycero-3-phosphocholine (DPPC) – were obtained from Avanti Polar Lipids in the lyophilized powder form and used without further purification.

Solid-state NMR. $\{^{15}\text{N}\}\text{HZ}$ was reconstituted into mechanically oriented DMPC bilayers at a peptide/lipid molar ratio (P/L) of 1/100. Ca. 30 mg of the MeOH co-solubilized peptide/lipid mixture were spread over 20 glass slides (7.5 mm \times 18 mm \times 0.06 mm) and the resulting films dried under vacuum. The slides were stacked and hydrated by incubation in 96% relative humidity at 48 °C overnight. The sample was wrapped in parafilm and a plastic foil to prevent drying.

Solid-state NMR (ssNMR) experiments were performed on an Avance III Bruker NMR spectrometer equipped with a 14.1 T widebore magnet. ^{31}P ssNMR spectra were acquired

at 242.9 MHz, using a Bruker flat-coil double-resonance $^1\text{H}/\text{X}$ probe, with a Hahn echo sequence (90° pulse of $5\ \mu\text{s}$; echo delay of $30\ \mu\text{s}$), employing ^1H SPINAL64 decoupling scheme during acquisition (decoupling strength 50 kHz). At least 256 scans were accumulated (acquisition time of 10 ms; recycle delay of 2 s). For ^{15}N -NMR, ^1H - ^{15}N cross-polarization experiment using a CP-MOIST pulse sequence was performed at 60.8 MHz. The experiments were accomplished using a locally built double-tuned probe with a low-E flat-coil resonator, employing a ^1H and ^{15}N radiofrequency field strength of 65 kHz during the cross-polarization, and a 36 kHz ^1H SPINAL16 decoupling during acquisition. A mixing time of $250\ \mu\text{s}$ was used, and 25600 scans were accumulated (acquisition time of 10 ms; recycle delay of 3 s). The ^{15}N chemical shift was referenced using the signal of a dry powder of ammonium sulfate, of which the chemical shift was set to 26.8 ppm. All NMR experiments were performed at $35\ ^\circ\text{C}$, i.e. above the DMPC phase transition temperature.

Synchrotron radiation circular dichroism (SRCD) spectroscopy. Measurements were carried out on the UVCD-12 beamline at the ANKA synchrotron facility at KIT.¹⁴ For non-oriented CD, HZ was dissolved in 1:1 (vol.) mixture (50% TFE) of 2,2,2-trifluoroethanol and a salt-free 10 mM phosphate buffer (pH 7.4 at $25\ ^\circ\text{C}$) at the end concentration $8\ \text{mg}\cdot\text{mL}^{-1}$. The sample was placed in a Hellma $12.5\ \mu\text{m}$ thick circular CaF_2 cuvette. Three consecutive scans were collected and averaged at $30\ ^\circ\text{C}$. The scans were collected between 270 to 170 nm at a rate of $15\ \text{nm}\cdot\text{min}^{-1}$ with 0.5 nm intervals using 1.5 s dwell time and 1 nm bandwidth. After subtracting the baseline spectrum of the pure solvent, the averaged spectrum was converted to mean residue ellipticity. For oriented CD (SROCD), mixtures of HZ (ca. $8\ \mu\text{g}$) and respective lipid (strictly $200\ \mu\text{g}$) at P/L of 1/100 were prepared first as $\text{MeOH}/\text{CHCl}_3$ solutions. The solutions were allowed to dry on quartz glass plates, placed into a locally built SROCD sample cell and hydrated by incubation in 97% relative humidity overnight. One scan running at $15\ \text{nm}\cdot\text{min}^{-1}$ with 0.5 nm intervals using 1.5 s dwell time and 1 nm bandwidth for each of the eight 45° rotation positions from 0° to 315° was collected. The data were acquired from 270 to 175 nm at $30\ ^\circ\text{C}$ under constant 97% relative humidity.

D. Additional HREX simulation

An additional HREX simulation was performed, starting from a different initial structure where the HZ molecule was placed in the aqueous phase. The HREX simulation ran for 1 μ s, and involved 8 replicas with the scaling factors were in the interval 1...0.5, corresponding to effective temperatures from 300 K to 600 K. The cut-off distance for Lennard-Jones interactions was increased to 1.4 nm in this simulation.

E. Additional – Metadynamics Simulation

Metadynamics simulations,¹⁵ optionally in its well-tempered variant,¹⁶ were performed with Plumed 2.1.2 interfaced to Gromacs 5.0. The molecular mechanics parameters were the same as used for the free MD and HREX simulations, as were the initial positions and orientations (HZ placed outside the DMPC bilayer, with its axis parallel to the bilayer surface). The collective variables z and τ were considered, much the same as in the HREX simulations.

In the normal metadynamics simulations, Gaussian potentials of 1.5 kJ·mol⁻¹ height were deposited every 1 ps or every 2 ps. The well-tempered metadynamics used two different values of the bias factor, 6 and 10, and Gaussians were deposited every 2 ps with an initial height of 1.2 kJ·mol⁻¹. For all of the simulations, the Gaussian width was set to 0.35 rad for τ and to 0.35 nm for z .

In all of the attempts, one of four different initial conformations of the peptide were employed: α -helix, 3_{10} -helix, fully extended and central- α . The first three structure were built according to the Methods section of the main text. The “central- α ” conformation was constructed by modelling only the central part of the peptide in an α -helical conformation; that involved only two hydrogen bonds, Ile3–Leu7 and Ile4–Leu8. The considered hydrogen bonds were restrained during the entire simulations. This unusual conformation was motivated by preliminary NMR results.

F. Additional – Umbrella Sampling Simulation

One-dimensional umbrella sampling (US) simulations were employed to estimate the free energy, or potentials of mean force (PMF) along the distance in the z -direction of the center of mass (COM) of the HZ molecule from COM of the bilayer. This variable describes the transfer of the HZ molecule from the DMPC bilayer to the aqueous phase, and also from one bilayer/solvent interface to the center of the bilayer.

The range of the z -coordinate from 0 (corresponding to the center of the bilayer) to 30 Å (which is already far in the aqueous phase) was divided into 61 windows spaced by 0.5 Å. Two series of US simulations were performed, with different starting coordinates in all of the windows. In the first set, the starting structures were created by pulling COM of HZ placed initially in the center of the bilayer (I-state) along the z -direction. In the second set, the initial pulling simulation was started with the HZ molecule placed at the edge of the hydrophobic tail region parallel to the surface (S-state). The initial structures of the I- and S-states were taken from the output of the previously performed free MD simulations. Harmonic biasing potential with a force constant of $10 \text{ kJ mol}^{-1} \text{ \AA}^{-2}$ was applied, and the simulation in each of the windows ran for 500 ns. The Gromacs `g_wham` tool was used to analyze the trajectories and construct the PMF.

II. RESULTS

A. Free simulation

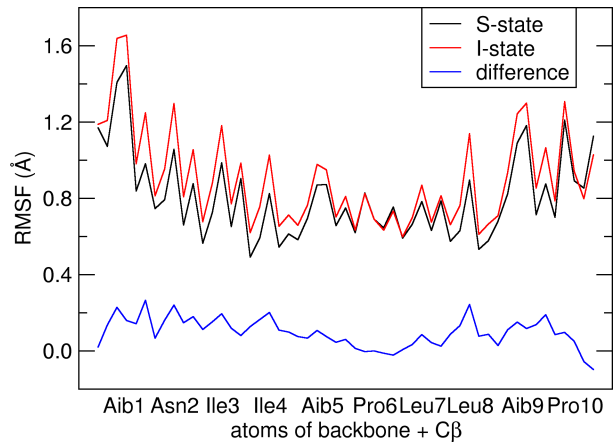


FIG. 1. Root mean square fluctuation (RMSF) of the individual atoms of backbones and $C\beta$ of the HZ molecule in the S- and I-states, obtained from free MD simulations.

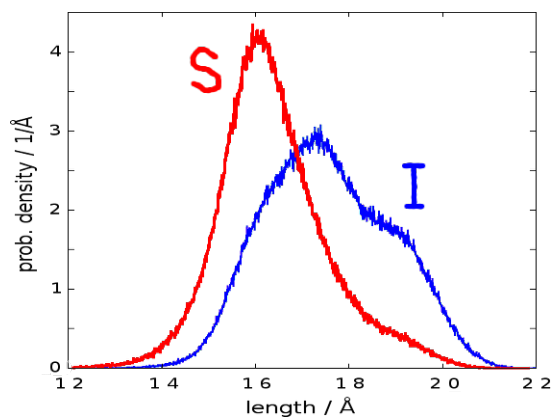


FIG. 2. Distribution of end-to-end length of the HZ molecule measured as the distance of the C_α of the first AA (Aib1) and the C_α of the last AA (Leu11) in the MD trajectories of the S and I orientations.

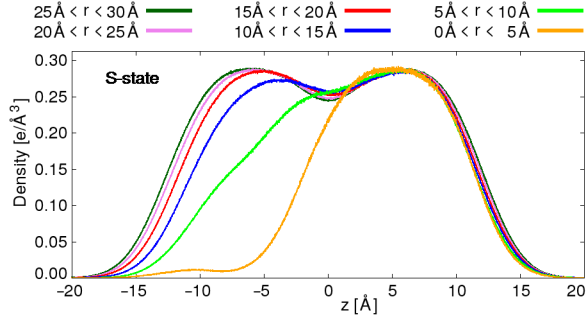


FIG. 3. Density profiles of the non-polar hydrocarbon tails of DMPC in the simulation of HZ in the S-state. The different profiles were obtained considering lipid atoms in the given ranges of horizontal distances from the center-of-mass of the HZ molecule. (Horizontal distance is the distance projected in the plane of bilayer surface.)

	S-state		I-state	
	φ	ψ	φ	ψ
Aib1	-46°	-16°	-62°	-17°
Asn2	-65°	-22°	-71°	-25°
Ile3	-69°	-30°	-68°	-26°
Ile4	-86°	-31°	-83°	-15°
Aib5	-57°	-26°	-57°	-23°
Pro6	-61°	-23°	-61°	-15°
Leu7	-71°	-26°	-62°	-16°
Leu8	-99°	-17°	-76°	-14°
Aib9	-59°	-21°	-59°	-22°
Pro10	-66°	-20°	-68°	-14°

TABLE II. Backbone dihedral angles of the dominant conformations of HZ observed in the unrestrained simulations of HZ immersed in the DMPC bilayer. Structures within 0.15 of each of the first two principal components were selected from the projection of each trajectory on the components obtained from principal component analysis performed on the combined trajectories. Presented are the averaged values of (φ, ψ) in these structural ensembles.

Root-mean-squared displacements of atomic positions (RMSD) of HZ with respect to static, idealized conformations were calculated along the MD trajectories. The idealized structures were $(\varphi, \psi) = (-74^\circ, -4^\circ)$ for 3_{10} , $(\varphi, \psi) = (-57^\circ, -47^\circ)$ for α , and considering the values of angles from Ref. 13 for β -bend ribbon. Only the fragment of the HZ molecule that may form a β -bend ribbon, consisting of the AAs Ile3–Pro10, was considered for this analysis, which was further restricted to the heavy atoms of the backbone.

reference	S-state	I-state
3_{10} -helix	1.25 ± 0.27	0.93 ± 0.30
β -bend ribbon	1.07 ± 0.24	1.10 ± 0.26
α -helix	1.40 ± 0.24	1.51 ± 0.28
average structure ^a	0.52 ± 0.20	0.58 ± 0.20

TABLE III. Root-mean-squared deviation (RMSD, in Å) of atomic positions of the HZ molecule with respect to selected reference structures, obtained from the MD trajectories with HZ molecule in the S and I orientations. The calculation of RMSD involved non-hydrogen atoms of the backbones of AAs 3 through 10. ^a Average structure taken from each respective MD trajectory.

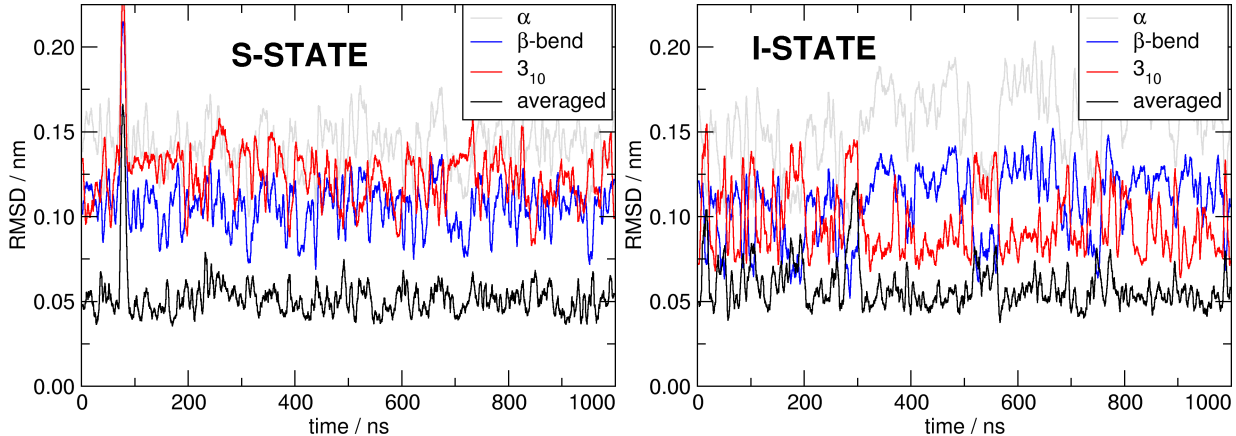


FIG. 4. Time course of RMSD of the HZ molecule with respect to the selected reference structures, in the unrestrained simulations of the S-state (left) and the I-state (right). The calculation involved the heavy atoms of the backbones of amino acids 3 through 10.

B. Free simulation – convergence of HZ structure

A principal component analysis (PCA) was performed on the structural ensemble of the HZ molecule that was obtained by combination of the MD trajectories generated previously for HZ in the S- and I-states (1 μ s each). Then, each of the two trajectories was projected into a two-dimensional space spanned by the first (PC1) and second eigenvectors (PC2) obtained from the PCA, see Fig. 5 for the projections. Note that the combination of PC1 and PC2 covers 72 % of structural variation of HZ in the structural ensemble combined from the simulations of S- and I-states. Also, we introduce a transformation of PC1 and PC2 into polar coordinates, as depicted in Fig. 5 also.

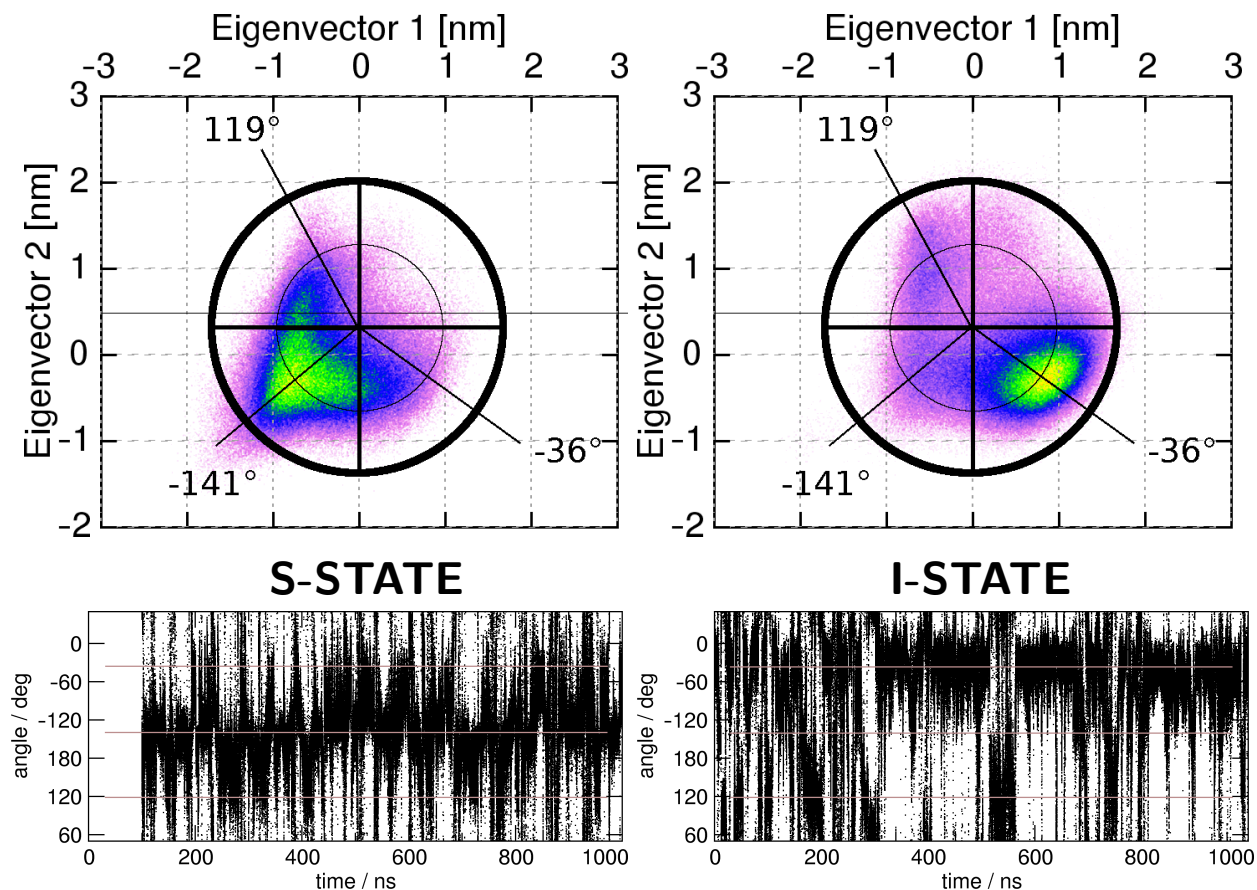


FIG. 5. Results from the principal component analysis. Top: Projection of each trajectory onto the first two eigenvectors, which were obtained from a PCA on the combined trajectories for the S- and I-states; Definition of the angular coordinate composed of PC1 and PC2, which makes it possible to distinguish between three structural states. Bottom: Time course of the angular coordinate in each of the trajectories.

The PCA plots reveal three different structural domains. Then, the structure at -141° is dominant in the S-state, and the structure at -36° dominates in the I-state, while the third structure at 119° is minor in both states. We use the angular coordinate obtained from PC1 and PC2 to assess the convergence of HZ structure in the free MD simulations performed.

On the assumption that three structural domains are possible, as identified above, it shall be checked whether interconversions between them are observed during the simulation period. To this end, the angular coordinate is plotted along the respective MD trajectories in Fig. 5 (bottom). For the S-state, there are a number of transitions between -141° and -36° , and 119° is populated transiently. The histogram of PC1/PC2 for the I-state features more clearly separated maxima, and the transitions between them are correspondingly more scarce; still, the dominantly populated -36° is interrupted by interconversions to -141° and 119° on multiple occasions. These observations confirm that the structural ensembles of HZ in the bilayer in both the S- and I-states are largely converged on the simulated time scale of $1 \mu\text{s}$.

C. HREX simulation – convergence of orientation of HZ in the bilayer

Several interconversion between the S- and I-states are observed in the HREX simulation of $2 \mu\text{s}$. This seems to be enough to provide a qualitatively correct free energy landscape (as presented in the main text), but even longer time scales would be required to obtain a statistically converged result.

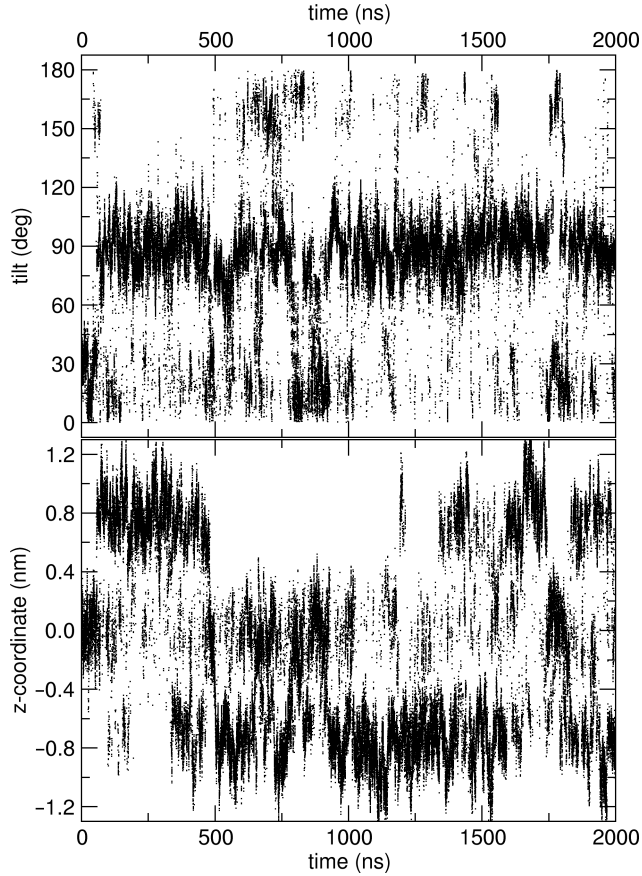


FIG. 6. The collective variables that describe the orientation of HZ in the DMPC bilayer, followed along the unperturbed replica ($\lambda = 1$) in the HREX simulation. The S-state is characterized by a tilt of 90° and z -coordinate of ca. $+0.8$ or -0.8 nm; the I-state exhibits a tilt close to 180° or -180° and z -coordinate of ca. 0.0 nm.

D. Additional HREX simulation

An additional HREX simulation was started with the HZ molecule located in the aqueous phase in all replicas, and the resulting free energy surface (FES) is shown in Fig. 7. Evidently, the deepest free energy minima are found in the aqueous phase, on both sides of the lipid bilayer. A minor minimum is found inside of the bilayer, corresponding to the S-state. In spite of the extended length of the simulations of 1 μ s, convergence has not been reached apparently, for two reasons: Firstly, the free energy plot should be symmetric, meaning that if one of the S-states (with $z \approx 8 \text{ \AA}$) was found, the other one ($z \approx -8 \text{ \AA}$) would be expected as well. And, more importantly, the HZ molecule in the aqueous phase is predicted as the most likely state, which is entirely unexpected considering the purely non-polar character of HZ.

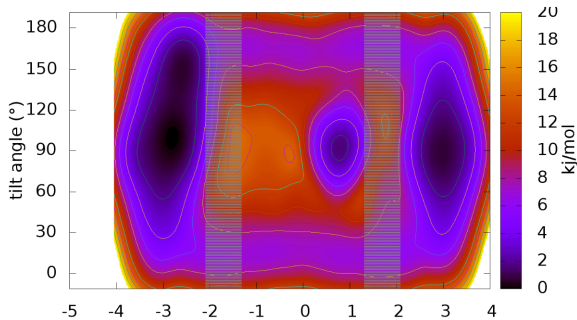


FIG. 7. Free energy surface from the HREX simulation with HZ molecule placed in the aqueous phase initially.

It seems that there is a rather high energy barrier opposing the insertion of HZ into the lipid bilayer, through the strongly polar lipid head group region. Then, the HZ molecule only passed into the hydrocarbon tail region late in the simulation, and the free energy minimum at $z \approx 8 \text{ \AA}$ is only shallow. Also, the extremely rare interconversion between solvent and lipid bilayer, which only took place once in only one of the replicas, means that it is extremely difficult if not impossible to reach convergence of the free energy profile.

E. Additional – Free energies from metadynamics simulations

Relative free energies of the various orientations of the peptide molecule in the bilayer represent some of the most desirable quantities in a study like this. Unfortunately, this goal is difficult to achieve even with extended sampling techniques. This is best illustrated by our application of metadynamics simulation, with the intention to reach convergence of free energies in a two-dimensional representation. The orientation of the HZ molecule is described with the z -coordinate and the tilt angle, much the same as in the HREX simulations presented in the main text. In recent work by other authors, metadynamics simulations have been successful in the reconstruction of water/membrane partitioning free energy surfaces, in particular for small solutes.^{17,18}

The same kind of calculation with a peptide, even a small one like HZ, in an atomistic lipid-water system is more challenging, and we are going to describe the problems that we were confronted with in these calculations. All of the attempted metadynamics simulations were either unstable or inefficient. Almost all of the normal metadynamics simulations crashed after ca. 100 ns. At this point, the underlying free energy surface was already filled with biasing Gaussians largely, and in fact, the motion along the collective variables (CV) became diffusive, see e.g. Fig. 8. A possible cause of the problem may lie in the singularities of the tilt angle at 0° and 180° ; the diffusive dynamics along tilt may have led to an accelerated motion along the tilt CV and instabilities whenever the tilt became close to 0° or 180° . Unfortunately, even an analysis performed for the period of simulation preceding the crash never produced any reliable free energy surfaces.

The well-tempered metadynamics simulations behaved somewhat better, but still no convergence was reached. The bias deposition rate decreased over simulation time, and probably the bias factors used were too low, so that the system was unable to explore all of the FES. Changing the bias factor value from 6 to 10 did not bring any improvement, and it is difficult to choose the suitable bias factor because the relevant barrier heights are unknown. Still, the best results from the many attempts exhibited two minima associable to the S- and I-states, see Fig. 9.

There might be various reasons for such unsatisfactory results. The first concerns the representation of the two CVs. The tilt angle as defined here exhibits singularities at 0° and 180° . While this is no problem in a post-processing of a free or HREX simulation,

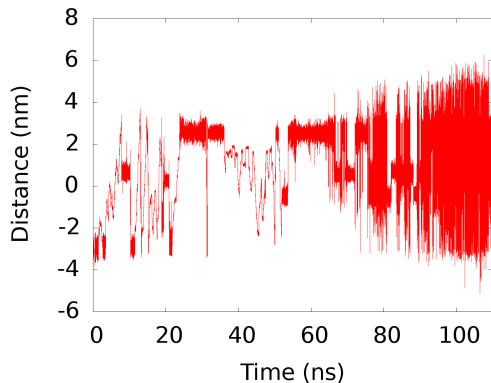


FIG. 8. Motion of the z CV during one of the normal metadynamics simulations of unrestrained HZ in a DMPC bilayer. The motion becomes diffusive after ca. 70 ns.

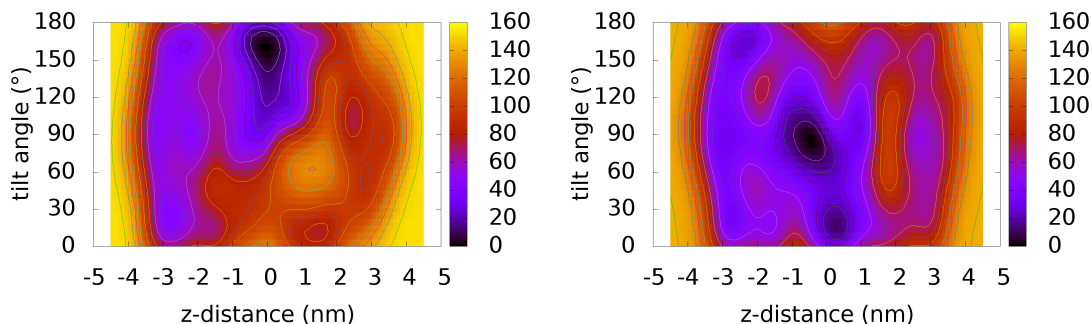


FIG. 9. Free energy surface from metadynamics well-tempered simulations with HZ molecule 3_{10} -helix restrained. The bias factor was set to 6 (left) and 10 (right).

it might become critical in a simulation with biasing potentials like metadynamics. A somewhat better choice might be the cosine of the tilt angle, and our further studies go in that direction. passing to the z -distance, this was defined relative to COM of all of the lipid. Such a definition may clearly lead to artifacts due to the undulations of the bilayer, which generate local deformations. Then, the COM of the entire bilayer does not describe the local neighborhood of the HZ molecule effectively. A better definition might be based on the lipid atoms within a cylinder aligned along the bilayer normal and centered on the solute.¹⁹

As mentioned above, even though the well-tempered simulations did not reach convergence, we were able to sample two minima of the FES, Surprisingly, only the peptide re-

strained to 3_{10} -helical conformation entered the hydrophobic region of the bilayer and really reached these minima. This means that the conformation of the peptide may be another important degree of freedom. Importantly, a dangerous caveat of metadynamics is that whenever such degrees of freedom, which are orthogonal to the biased CVs, are not sampled properly then the convergence becomes difficult, possibly leading to incorrect free energies.

In addition, another important phenomenon that is uncontrolled in the metadynamics simulation is the deformation or disruption of the bilayer that takes place as the peptide is being transferred from the aqueous phase to the interior of the bilayer. It seems to be very difficult to define a CV to control such structural changes, while it would be clearly orthogonal to the existing CVs, in the metadynamics language. A possible solution to that issue could be to combine metadynamics (with the present CVs) with HREX.

F. Additional – Free energies from umbrella sampling simulations

In another attempt to estimate free energies, we resorted to a one-dimensional representation and performed umbrella sampling simulations. The aim was to obtain the free energy profile for the HZ molecule approaching the center of the lipid bilayer and, on the other hand, being pulled out across the polar head-group layer into the aqueous solvent. The reaction coordinate was represented by the difference of the z -coordinate of COM of HZ and the z -coordinate of COM of the lipid bilayer. Two series of simulations were performed, each starting in one of the previously identified stable orientations of HZ, the S- and I-states. For each of the series, the reaction coordinate was divided into 60 windows spaced by 0.5 Å, and the starting structures for each of the windows were created from the respective stable state (S or I), by means of a rather fast non-equilibrium pulling simulation. Thus, the starting structures in each of windows were different in the S- and I-series of US simulations. It will turn out that this is an important point.

The free energy plots shown in Fig. 10 originate in series of US simulations of 500 ns per window, or 30 μ s in total, for each of the I- and S-series. Apparently, even such an extensive sampling is insufficient to obtain a result that would be converged in the hydrocarbon tail region of $z = 0 - 1$ Å. The reason is that the orientation of the HZ molecule hardly changes during a simulation in a given window, and no interconversions between the S- and I-states are observed. Thus, each of the two series of US simulations provide its respective starting

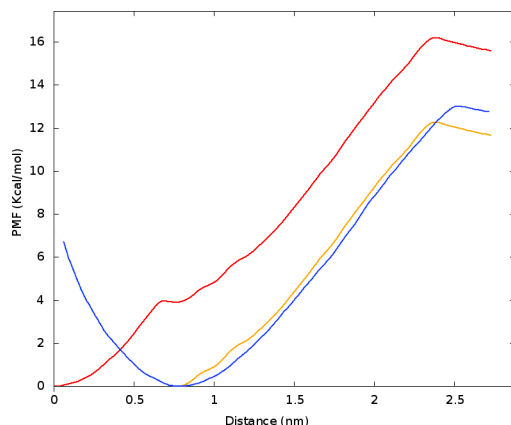


FIG. 10. Free energy profiles obtained from 1D umbrella sampling simulations of pulling HZ out of the bilayer into the aqueous phase. Starting structures generated by pulling simulations from two different structures; Red – starting from the I-state; orange – the same data, shifted vertically; blue – starting from the S-state.

structure as the more stable state – just because the respective other state is not sampled correctly.

On the other hand, both free energy profiles are very similar in the range of reaction coordinate above 10 Å. Seemingly, this provides a certain confidence to a rough estimate of the free energy cost of pulling the HZ molecule out of the membrane into the aqueous phase, which is around 11–13 kcal/mol on the basis of the US simulations performed. It would little surprise that such a largely non-polar molecule like HZ prefers the non-polar environment of the hydrocarbon tails to the polar solvent strictly. However, there might be a very similar problem as in the above reported metadynamics simulations – the deformation of the bilayer possibly leading to poor convergence, and thus to wrong free energies and hysteresis.

REFERENCES

- ¹Bayly, C. I., P. Cieplak, W. D. Cornell, and P. A. Kollman, 1993. A well-behaved electrostatic potential based method using charge restraints for deriving atomic charges: The RESP model. *J. Phys. Chem.* 97:10269–10280.
- ²Frisch, M. J., G. W. Trucks, H. B. Schlegel, G. E. Scuseria, M. A. Robb, J. R. Cheeseman, G. Scalmani, V. Barone, B. Mennucci, G. A. Petersson, H. Nakatsuji, M. Caricato, X. Li, H. P. Hratchian, A. F. Izmaylov, J. Bloino, G. Zheng, J. L. Sonnenberg, M. Hada, M. Ehara, K. Toyota, R. Fukuda, J. Hasegawa, M. Ishida, T. Nakajima, Y. Honda, O. Kitao, H. Nakai, T. Vreven, J. A. Montgomery, Jr., J. E. Peralta, F. Ogliaro, M. Bearpark, J. J. Heyd, E. Brothers, K. N. Kudin, V. N. Staroverov, R. Kobayashi, J. Normand, K. Raghavachari, A. Rendell, J. C. Burant, S. S. Iyengar, J. Tomasi, M. Cossi, N. Rega, J. M. Millam, M. Klene, J. E. Knox, J. B. Cross, V. Bakken, C. Adamo, J. Jaramillo, R. Gomperts, R. E. Stratmann, O. Yazyev, A. J. Austin, R. Cammi, C. Pomelli, J. W. Ochterski, R. L. Martin, K. Morokuma, V. G. Zakrzewski, G. A. Voth, P. Salvador, J. J. Dannenberg, S. Dapprich, A. D. Daniels, O. Farkas, J. B. Foresman, J. V. Ortiz, J. Cioslowski, and D. J. Fox. Gaussian 09 Revision C.01. Gaussian Inc. Wallingford CT 2009.
- ³Darden, T., D. York, and L. Pedersen, 1993. Particle mesh Ewald – an $n \cdot \log(n)$ method for Ewald sums in large systems. *J. Chem. Phys.* 98:10089–10092.
- ⁴Gromacs reference manual, version 2016, section 4.9.1. <http://manual.gromacs.org/documentation/2016/manual-2016.pdf>, last accessed 7 Sep 2016.
- ⁵Hess, B., H. Bekker, H. J. C. Berendsen, and J. G. E. M. Fraaije, 1997. LINCS: A linear constraint solver for molecular simulations. *J. Comput. Chem.* 18:1463–1472.
- ⁶Nosé, S., 1984. A molecular dynamics method for simulations in the canonical ensemble. *Mol. Phys.* 52:255–268.
- ⁷Hoover, W. G., 1985. Canonical dynamics: Equilibrium phase-space distributions. *Phys. Rev. A* 31:1695–1697.
- ⁸Nosé, S., and M. L. Klein, 1983. Constant pressure molecular dynamics for molecular systems. *Mol. Phys.* 50:1055–1076.
- ⁹Jämbeck, J. P. M., and A. P. Lyubartsev, 2012. Derivation and Systematic Validation of a Refined All-Atom Force Field for Phosphatidylcholine Lipids. *J. Phys. Chem. B*

- 116:3164–3179.
- ¹⁰Ulmschneider, J. P., J. C. Smith, M. B. Ulmschneider, A. S. Ulrich, and E. Strandberg, 2012. Reorientation and dimerization of the membrane-bound antimicrobial peptide PGLa from microsecond all-atom MD simulations. *Biophys. J.* 103:472–482.
- ¹¹Kandt, C., W. L. Ash, and D. P. Tieleman, 2007. Setting up and running molecular dynamics simulations of membrane proteins. *Methods* 41:475–488.
- ¹²2010. AmberTools 1.4. <http://ambermd.org>.
- ¹³Ségalas, I., Y. Prigent, D. Davoust, B. Bodo, and S. Rebuffat, 1999. Characterization of a type of β -bend ribbon spiral generated by the repeating (Xaa-Yaa-Aib-Pro) motif: The solution structure of harzianin HC IX, a 14-residue peptaibol forming voltage-dependent ion channels. *Biopolymers* 50:71–85.
- ¹⁴Bürck, J., S. Roth, D. Windisch, P. Wadhvani, D. Moss, and A. S. Ulrich, 2015. UV-CD12: synchrotron radiation circular dichroism beamline at ANKA. *J. Synchrotron Rad.* 22:844–852.
- ¹⁵Laio, A., and M. Parrinello, 2002. Escaping free energy minima. *Proc. Natl. Acad. Sci. USA* 99:12562–12566.
- ¹⁶Barducci, A., G. Bussi, and M. Parrinello, 2008. Well-Tempered Metadynamics: A Smoothly Converging and Tunable Free-Energy Method. *Phys. Rev. Lett.* 100:020603.
- ¹⁷Jämbeck, J. P. M., and A. P. Lyubartsev, 2013. Exploring the Free Energy Landscape of Solutes Embedded in Lipid Bilayers. *J. Phys. Chem. Lett.* 4:1781–1787.
- ¹⁸Bochicchio, D., E. Panizon, R. Ferrando, L. Monticelli, and G. Rossi, 2015. Calculating the free energy of transfer of small solutes into a model lipid membrane: Comparison between metadynamics and umbrella sampling. *J. Chem. Phys.* 143:144108.
- ¹⁹Filipe, H. A. L., M. João Moreno, T. Róg, I. Vattulainen, and L. M. S. Loura, 2014. How To Tackle the Issues in Free Energy Simulations of Long Amphiphiles Interacting with Lipid Membranes: Convergence and Local Membrane Deformations. *J. Phys. Chem. B* 118:3572–3581.